INÊS FERNANDES MENDES

CHARACTERISATION AND ASSESSMENT OF LUMBAR DISC HERNIATION USING IMAGE SEGMENTATION AND MODELLING

Biomedical Engineering Master's Dissertation Report

Supervisor
Professor Doutor André Castro

Co-supervisors
Professora Doutora Rita Fernandes
Dr. Nuno Cristino

December 2024

HOSPITAL DA LUZ

INÊS FERNANDES MENDES

CHARACTERISATION AND ASSESSMENT OF LUMBAR DISC HERNIATION USING IMAGE SEGMENTATION AND MODELLING

Jury

President: Professor Doutor Célio Pina, Escola Superior de Tecnologia de Setúbal, Instituto Politécnico de Setúbal

Supervisor: Professor Doutor André Castro, Escola Superior de Tecnologia de Setúbal, Instituto Politécnico de Setúbal

Vowel: Professor Doutor Nuno Matela, Faculdade de Ciências da Universidade de Lisboa

December 2024

Acknowledgments

I would like to begin by expressing my gratitude to the Instituto Politécnico de Setúbal for being a strong force for fostering a culture of entrepreneurial and research culture, and for providing the opportunity to study for a Master's degree in Biomedical Engineering. These 5 years of higher education, have allowed me to grow significantly, both personally and academically. I have developed a continuous desire to learn more and have improved my ability to persist in the face of various challenges.

A special thanks to the supervisor and co-supervisors of this project, Prof. André Castro, Prof.ª Rita Fernandes and Dr. Nuno Cristino, for their teaching, understanding and knowledge sharing, which greatly contributed to the success of this project.

My sincere thanks to Prof. André Castro for all the insights, suggestions and sharing of ideas that contributed to the success of this work. I would also like to thank him for his unconditional support, vast knowledge and patience, without which none of this would have been possible.

I would especially like to thank Dr. Nuno Cristino for all the knowledge, availability, support and time dedicated to the success of this work. I would also like to thank Technician Carlos Martinho and nurses Marisa Oliveira e Mafalda Branco for their assistance throughout this process, as well as all the staff for their kindness and help. A sincere thank you to Hospital da Luz de Setúbal for their availability and ability to receive students for the development of a Master's Dissertation.

Finally, I would like to express my sincere gratitude to all my friends and colleagues who supported me, directly or indirectly, in the completion of this project, especially Margarida Pedrosa and Ana Filipa Aguiar for their interest in the subject and the assistance they provided.

In conclusion, my most sincere thanks go to my family for their strength, patience and unconditional support over the years and for always believing in me and my abilities in order to achieve all the success I desired.

Resumo

A hérnia discal lombar é o diagnóstico mais comum entre as doenças degenerativas da coluna lombar. Manifesta-se habitualmente por dor lombar (lombalgia) e dor irradiada nas pernas (ciatalgia) e pode estar associada a distúrbios sensoriais e motores, que por sua vez afetam a qualidade de vida do doente. O tratamento pode incluir uma combinação de terapêutica farmacológica, reabilitação ou até procedimentos cirúrgicos, sendo uma das cirurgias da coluna vertebral mais frequentes. A decisão de alocação para cada grupo de tratamento, depende dos parâmetros clínicos como dor, limitação de movimento, incapacidade funcional e qualidade de vida. Os exames imagiológicos permitem comprovar a existência de uma hérnia e a compressão que esta exerce sobre um nervo. Este trabalho pretende correlacionar os parâmetros clínicos, os parâmetros quantitativos e qualitativos das várias modalidades de imagem e os parâmetros quantitativos dos modelos 3D, em pacientes com hérnia discal lombar manifestada como ciática aguda.

O estudo incluiu um conjunto de 10 pacientes recrutados na consulta externa do Serviço de Neurocirurgia do Hospital da Luz Setúbal. Para cada paciente, foi verificado se o mesmo possuía um exame de Ressonância Magnética (MRI), Tomografia Computadorizada (CT), Raios-X e Raios-X Funcional, para que pudessem ser medidos parâmetros através dessas modalidades de imagem. Por fim, foram segmentados modelos 3D da coluna lombar dos pacientes que possuíam uma CT.

Os resultados obtidos mostram que as características clínicas, como sexo, idade, IMC, ODI e NPRS não apresentam uma correlação evidente com a área da hérnia. A altura do disco, altura da vértebra, ângulo intervertebral e ângulo de lordose lombar foram os parâmetros quantitativos analisados com maior detalhe. Desta forma, verificou-se que de maneira geral, as combinações de MRI com CT e modelos 3D apresentaram valores consistentes com a literatura, ao contrário do MRI com Raios-X e Raios-X Funcional.

Assim, concluiu-se que o MRI, CT e modelos 3D são os mais semelhantes entre si em termos das medições dos parâmetros. Por outro lado, as medições realizadas em Raios-X e Raios-X Funcional diferem das obtidas em MRI e CT, devido à variação na postura durante a aquisição das imagens.

Palavras-chave: Coluna lombar, lombalgia, ciatalgia, hérnia discal lombar e segmentação de imagem.

Abstract

Lumbar disc herniation is the most common diagnosis among degenerative diseases of the lumbar spine. It usually manifests as low back pain and radiating leg pain (sciatica) and may be associated with sensory and motor disturbances, which in turn affect the patient's quality of life. Treatment may include a combination of pharmacological therapy, rehabilitation or even surgical procedures, with spinal surgery being one of the most common. The decision to allocate a patient to a specific treatment group depends on clinical parameters such as pain, movement limitation, functional disability and quality of life. Imaging exams can confirm the existence of a herniation and the compression it exerts on a nerve. This study aims to correlate clinical parameters, qualitative and quantitative parameters from various imaging modalities and the quantitative parameters of 3D models in patients with lumbar disc herniation manifesting as acute sciatica.

The study included a group of 10 patients recruited from the Neurosurgery Department of the Hospital da Luz de Setúbal. For each patient, it was verified whether they had a Magnetic Resonance Imaging (MRI), Computed Tomography (CT), Standing X-ray and Functional X-ray, in order to measure parameters using these imaging modalities. Finally, 3D models of the lumbar spine were segmented for patients who had a CT scan available.

The outputs obtained show that clinical characteristics such as sex, age, BMI, ODI and NPRS do not exhibit a clear correlation with the hernia area. Disc height, vertebra height, intervertebral angle and lumbar lordosis angle were the quantitative parameters analysed in the greatest detailed. As a result, it was found that combinations of MRI with CT and 3D models showed values consistent with the literature, unlike the combinations of MRI with Standing and Functional X-ray.

Thus, it was concluded that MRI, CT and 3D models are the most similar to each other in terms of parameter measurements. On the other hand, the measurements obtained from Standing and Functional X-ray differ from those obtained from MRI and CT, due to variations in posture during image acquisition.

Keywords: Lumbar spine, low back pain, sciatica, lumbar disc hernia and image segmentation.

Contents

List of Figures

List of Tables

List of Acronyms and Abbreviations

AF	Annulus Fibrosus
BMI	Body Mass Index
CT	Computed Tomography
DB	Database
HLS	Hospital da Luz de Setúbal
IVD	Intervertebral Disc
LBP	Low Back Pain
LDH	Lumbar Disc Herniation
MRI	Magnetic Resonance Imaging
NP	Nucleus Pulposus
NPRS	Numerical Pain Rating Scale
ODI	Oswestry Disability Scale
2D	Two-dimensional
3D	Three-dimensional

List of Symbols

°	Degree
=	Equal
>	Greater than
≥	Greater than or equal to
kg	Kilogram
kg/m^2	Kilogram per square meter
≤	Less than or equal to
<	Less than
m	Meter
mm	Millimetre
%	Percentage
±	Plus or minus
mm^2	Square millimetre

1. Introduction

Low back pain (LBP) is a recurring symptom that can be related to different lumbar spine pathologies and significantly affects the quality of life of thousands of people around the world [1]. Individuals affected by LBP have a reduced quality of life and in many cases leads to loss of working hours and early retirement. Sciatica refers to a condition characterised by pain radiating along the lower limb following the sciatic nerve anatomy, which runs from the lower back, through the buttocks and hips, down to the legs. Sciatic pain usually occurs on only one side of the body and can range from mild to intense [2].

Lumbar disc herniation (LDH) is the most common diagnosis among degenerative anomalies of the lumbar spine, with a typical clinical condition that includes initial LBP followed by sciatica [3]. Although symptoms and severity may vary, lumbar degenerative diseases, such as LDH, are theoretically associated with biomechanical deficiencies in the spinal muscles, resulting in inefficient and energy-consuming gait patterns and subsequently, a deterioration in the quality and capability of walking [4]. Other symptoms, such as LBP and radiating leg pain, can affect the patient's daily activities and quality of life [5]. The prognosis for patients with acute sciatica is generally favourable, with most cases resolving in less than 4 to 6 weeks, without long-term complications, although 20-30% of patients still experience pain after 1 year [6], [7].

LDH, one of the main causes of LBP, is the displacement of the nucleus pulposus (NP) beyond normal limits of the annulus fibrosus (AF), due to a combination of external forces and degenerative changes in the lumbar disc [5]. It is the most common diagnosis among degenerative abnormalities of the lumbar spine (affecting 2 to 3% of the population) and is the main cause of spinal surgery in the adult population [3].

Starting from medical imaging methods, such as Magnetic Resonance Imaging (MRI) or Computed Tomography (CT), it is possible to develop a three-dimensional (3D) reconstructions of the functional units of the lumbar spine (3D models), enhancing its characterisation and disease diagnosis [8].

1.1 Motivation

This work was proposed by Dr. Nuno Cristino, a neurosurgeon at the Hospital Da Luz de Setúbal (HLS) and is focused on the search for significant advances in the understanding and approach to LBP. The motivation for this study lies in the need to improve the assessment and treatment of clinical situations related to the lumbar spine, which significantly impact the quality of life of many individuals. In this way, the use of computational modelling is increasing exponentially, as it allows a detailed analysis of different clinical and biomechanical scenarios. Thus, this work aims to contribute for a better understanding of specific LBP, as well as to improve the well-being of patients affected by this condition.

1.2 Objectives

This study aims to correlate clinical characteristics, quantitative and qualitative parameters from various imaging modalities, and quantitative parameters from 3D models in patients with LDH manifested as acute sciatica. Additionally, the study aims to characterise baseline clinical characteristics and imaging parameters, in patients with LDH manifested as acute sciatica, as well as correlate them with patient's response to treatment.

Given this, defining the basic clinical characteristics and neuroimaging markers associated with the patient's evolution, will contribute for a more standardised approach to conservative treatment versus surgical planning, with a better transition to minimally invasive procedures, reduced risks, lower costs and maximised clinical outputs.

2. Literature review

2.1 Anatomy of the vertebral column

The vertebral column is the central support structure of our body, which allow us to stand upright due to the connections between the different parts of the skeleton. The spine supports the weight of the head and trunk, as well as allow their movement (flexion, extension and rotation); protects the spinal cord; allows the spinal nerves to exit the spinal canal and provide a place for muscles to be inserted. This structure is made up of 33 bones and is divided into 5 regions: cervical, thoracic (dorsal), lumbar, sacrum and coccyx. In addition, the spine has 4 curvatures, 2 convex towards the front, known as lordosis (cervical and lumbar) and 2 concave towards the front, known as kyphosis (thoracic and sacral) [9], [10].

2.1.1 Vertebrae

The bone components that make up the spine are called vertebrae, and they differ slightly depending on the spine segment they belong to. Each vertebra consists of a body, an arch and processes. The body of the vertebrae supports the weight and has a cylindrical shape. Adjacent vertebrae are separated by the intervertebral disc (IVD). The vertebral canal contains and protect the spinal cord (tubular nerve tissue). The vertebral arch is made up of two pedicles, which connect the posterior arch to the body and two lamina that extend from the pedicle to join the spinous process. The pedicles contain vertebral notches that form intervertebral foramina, which serve to facilitate the passage of the spinal nerves from the spinal cord to the paravertebral space. Finally, the bone processes can be divided into transverse processes, spinous processes and articular processes. The spinous and transverse processes are connection points for the back muscles, while the superior and inferior articular processes establish connections with the inferior articular processes of the vertebrae above and the superior articular processes of the vertebrae below, respectively [9].

The vertebrae are composed, on the outer layer, of cortical bone – dense and compact bone with a function of protection and structural support – and on the inner layer, of trabecular bone – porous bone with an important role in shock absorption and load distribution during physical activities [9].

The lumbar spine is composed of the L1 to L5 vertebrae. The lumbar vertebrae are known for having wide, thick bodies and strong, rectangular transverse and spinous processes. Additionally, one of their main characteristics is the orientation of the bone processes. Thus, the superior articular processes are oriented inward, while the inferior articular processes are oriented outward, which increases the strength of the lower spine and limits its rotation. The L5 vertebrae is the largest vertebrae in the human body and, as such, supports and transmits body weight to the base of the sacrum [9]. Figure 2.1 shows the structure of the lumbar spine and the components of each vertebra.

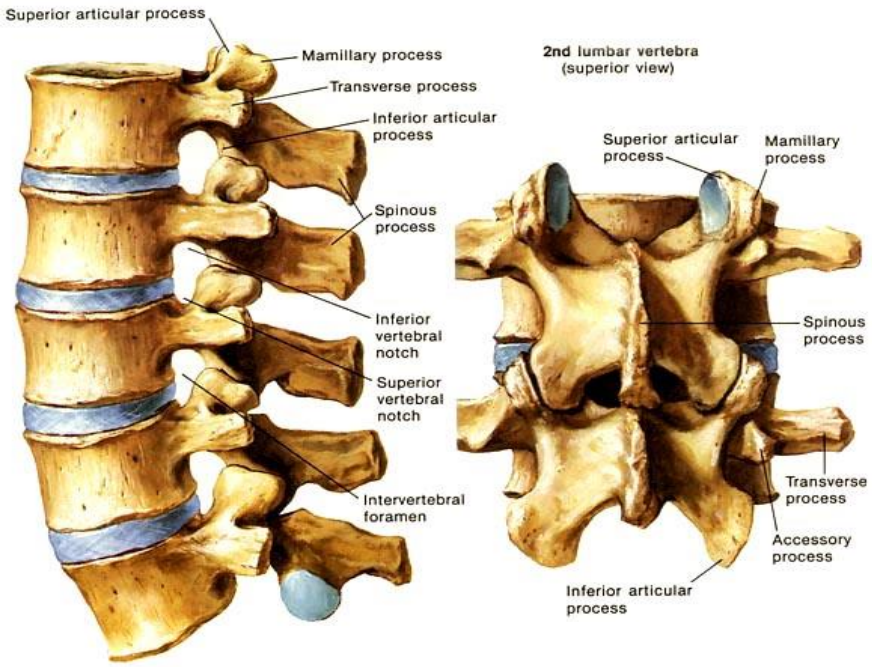

Figure 2.1 – Left: Lumbar vertebrae, Right: 3rd and 4th lumbar vertebrae [11].

2.1.2 Intervertebral discs

The IVDs are cartilaginous avascular structures located between the vertebrae and are made up of an AF on the outside and a NP on the inside. These structures serve to provide cushioning, stability and flexibility to the spine, in order to prevent friction and allow a small degree of flexibility between the vertebrae [10].

The AF is composed of several concentric layers of tough fibrous tissue. Each layer consists of collagen fibres arranged in different orientations to provide flexibility and stability to the structure. Due to its extensible characteristics and resistance to traction and compression, it

allows for torsional and shear movements. These fibres form a concentric outer layer and a circular inner layer in the AF, that gives multidirectional strength to the IVD. The vertebral bodies are covered on the top and bottom by an endplate to allow the IVD flexibility and adhesion during movement and absorption of resulting impacts. The endplates have two layers, a bone plate that connects to the vertebra and allows the passage of blood and nutrients to the IVD cells, and a cartilaginous plate which connects to the IVD. In addition, the AF acts as a barrier, keeping the NP from moving out of the centre of the IVD. However, due to the natural aging process and wear and tear, the AF can degenerate, increasing the risk of problems associated with the spine, such as LBP, among others [10].

The NP consists of a gelatinous and highly hydrated structure, as it is composed mainly of water. The high concentration of water in the NP allows it to act as a shock absorber, distributing compression loads that occur during daily activities and spinal movement, protecting the vertebrae and adjacent IVDs from the excessive wear and injury. It also helps maintain the proper height of the IVDs, which is crucial for spinal stability and alignment. An important feature of the NP is that it deforms under pressure, accommodate movement and transmit compressive loads between adjacent vertebrae. Over time, like the AF, the NP can naturally age and degenerate, which can result in water loss and a decrease in elasticity, leading to a decrease in damping capacity and an increased risk of back problems [10].

2.1.3 Joints and ligaments

In the vertebral column, there are several joints and ligaments that work together to maintain the stability of the spine and provide structural integrity and flexibility to the movement of the lumbar spine [12].

The facet of zygapophyseal joints are synovial joints located between the superior articular processes of one vertebra and the inferior articular processes of the adjacent vertebra and connect the vertebrae of the lumbar spine. These joints are covered by articular cartilage and are surrounded by a joint capsule containing synovial fluid, which provides lubrification and reduces friction during movement. When the facet joints of the spine are healthy, they maintain the stability of the lumbar spine while facilitating movements such as flexion, extension and abduction, but not rotation [12].

The fibrous ligaments present in the spine are divided into supraspinous ligaments, interspinous ligaments, flavum ligaments and intertransverse ligaments. The supraspinous ligament is characterised as bands of strong, dense fibrous tissue, which join the tips of the spinous processes and limit the flexion of the spine. The interspinous ligament is composed of fibrous tissue, which connects the spinous processes of adjacent vertebrae and limits flexion of the spine. The flavum ligament is a structure rich in elastin that lengthens and shortens depending according to flexion and extension movements, respectively, and connects the laminae of adjacent vertebrae and limits the flexion of the spine. The intertransverse ligaments connect the transverse processes of adjacent vertebrae and limit lateral flexion of the spine. In addition to the ligaments mentioned above, the bodies of the vertebrae have the anterior longitudinal ligament and the posterior longitudinal ligament, which are responsible for connecting the anterior and posterior surfaces, respectively, of all vertebral bodies along the spine and reinforcing the AF [12].

2.2 Degeneration of the lumbar spine

Spinal problems generally arise with the natural aging of the body, but they can also occur due to fractures, poor posture, excess weight, lack of physical activity, among other factors. Spinal problems can cause one or more symptoms such as back and neck pain, a tingling sensation, a reduction in normal range of movement, among others. As a result, some types of degenerative spinal pathologies can include spinal stenosis, abnormal curvatures of the lumbar spine, spondylitis, osteoporosis, IVD degeneration and spinal osteoarthritis. In various studies, it has been found that spinal degeneration is more prevalent in males compared to females [3].

LBP is a common clinical symptom that occurs predominantly in middle and old age and is characterised by pain in the lumbar spine, usually between the 12^{th} rib and the inferior gluteal folds, with or without leg pain [13]. This symptom is quite common and debilitating, with the pain ranging from mild to severe and varying in duration. LBP can be classified as acute (sudden onset and lasting less than 6 weeks), subacute (lasting between 6 and 12 weeks) or chronic (lasting longer than 12 weeks). This classification is important because it impact differently the patient and might be associated with different causes and treatment choices. The most concerning cases are those where symptoms do not improve after 3 months, those that do not respond to treatment and those that occur in patients with a history of serious diseases. LBP can

also be classified in specific and non-specific. The first is related to pathoanatomical causes, such as degenerative changes, systemic disease, infection, neoplasia, trauma or structural deformity [1], [14]. In the absence of a specific patho-anatomic diagnosis, approximately 90% of individuals with LBP are labelled as having "non-specific LBP" [15]. This condition typically arises from an imbalance between the spine's load-bearing demands and its capacity to handle them, leading to pain without structural changes in the lumbar spine [1], [14].

Sciatica, also known as sciatic pain, outputs from a pathology of the sciatic nerve or sciatic nerve root. It is a symptom caused by pain, weakness, numbness or tingling, that originates in the lumbar region and descends through the gluteal region to the posterior portion of the hip and leg, following the path of the sciatic nerve. This nerve is the longest in the human body, originates in the lumbar region of the spinal cord, from the nerve roots of L4 to S2 and ends in the posterior region of the leg, with branches extending to the foot. In most cases, sciatica is caused by a compression of the fifth nerve root (L5) or the first sacral nerve (S1). This symptom occurs when the contents of the IVD nucleus overflow and consequently compress the nerve roots that make up the sciatic nerve. The nerve roots become inflamed and irritated by the chemical substances that are released from the NP of the IVD and/or the mechanical effect of direct compression of the nerve. The pain the patient feels can be caused by the compression of the sciatic nerve inside or outside the spinal canal and the main causes are the appearance of an LDH, a muscle contracture around the sciatic nerve, compression of the spinal canal or the misalignment of a vertebra. Therefore, sciatic pain doesn't manifest immediately after a specific event or trauma, it mostly develops gradually. The symptoms depend on the type, location and severity of the condition causing the sciatica. Sciatica can be classified as based on intensity and duration of the symptoms [16], [17]. Most cases of sciatica resolve in less than 4 to 6 weeks, and it is recommended to start with conservative treatment (physiotherapy and medication), then move on to steroid injections, followed by surgery when non-surgical treatment is insufficient, and the patient is still in a lot of pain [18], [19]. Surgery for sciatica aims to decompress the nerve root by removing the LDH. The therapeutic role of discectomy is restricted to faster recovery, rapid relief of leg pain and improvement of disability [7]. Recurrent pain after lumbar discectomy can be due to a variety of causes, including a new LDH at other levels of the spine, segmental instability induced by partial removal of the posterior elements, or other anatomical changes involving the spinal canal in addition to the IVD [2], [20].

2.3 Lumbar Disc Herniation

LDH occurs when the contents of the IVD – NP – displace through its outer membrane – AF. Depending on the volume of herniated material, there may be compression and irritation of the nerve roots and dural sac, clinically represented by initial LBP, which may progress to sciatica [3].

Currently, LDH is the most common diagnosis among degenerative abnormalities of the lumbar spine and is the leading cause of spinal surgery in younger patients. This condition mainly appears between the ages of 40 and 50, although it can be seen in all age groups. This is because, during this age group, the IVDs begin to lose some of their flexibility and elasticity, making them more susceptible to injury. This condition manifests slightly more in males than females and may be due to differences in work or physical activities. Because it is so common, it has become a global health problem due to the disability it causes [3].

LDH causes limitation of movement or activities, such as lifting heavy objects or sitting for long periods of time. It can be associated with sensory or motor changes, and loss of bladder or bowel control. In this way, LDH can significantly affect people's quality of life and lead to emotional disorders such as anxiety and depression [3].

Imaging diagnosis of LDH is crucial to confirm the presence, location and severity of the LDH, as well as for evaluating potential compression of nerve structures and subsequently determine the most appropriate treatment, based on the surgeon's opinion. The preferred imaging method is MRI, as it provides a detailed view of the IVDs, spinal canal and nerve structures. In addition, dynamic test in flexion and extension are also performed as complementary assessments to obtain information regarding the biomechanics of the spine [3].

2.3.1 Classification and characterization of LDH

MRI can be used to classify LDHs qualitatively. LDH can be located at various levels between the vertebrae, and the same patient can have more than one herniated level. In terms of their location, LDHs can be ascending, descending or at the IVD level. An ascending LDH is located above the midline of the IVD, closer to the posterior limit of the vertebral body above the LDH. On the other hand, a descending LDH is located below the midline of the IVD, closer

to the vertebra below the LDH. Finally, a LDH at the IVD level is located at the midline of the IVD [21].

LDH are classified according to their type as follows [21]:

- Prolapse: The IVD moves slightly out of its normal space, but the AF remains intact.
- Protrusion: The NP pushes against the AF, without rupturing it, resulting in a localised bulge. The NP remains intact, but there is a loss of the oval shape. Base > Height.
- Extrusion: The NP breaks through the AF but is still contained by the posterior longitudinal ligament or another anatomical structure. The NP is deformed and suffers a "strangulation". Base < Height.
- Sequestration: A fragment of the NP completely breaks through the AF and separates from the main IVD, migrating into the spinal canal. The NP is significantly damaged and may divide into two parts.

Figure 2.2 shows an illustration of different types of LDH.

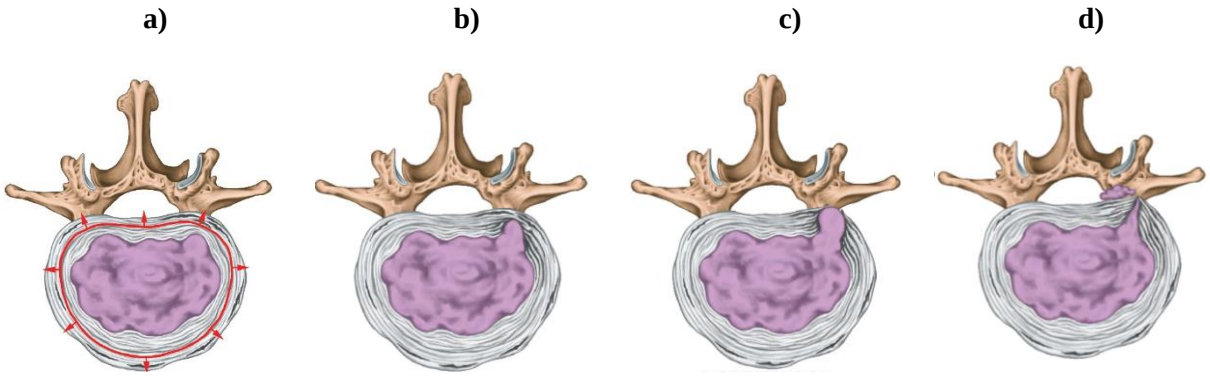

Figure 2.2 – Types of LDH: a) Prolapse, b) Protrusion, c) Extrusion and d) Sequestration [22].

In addition, it is necessary to characterise LDHs according to their topography, considering their location in relation to the central axis (midline) of the spine in [21]:

- Median: The LDH arises directly in the posterior midline of the IVD, protruding into the centre of the spinal canal.
- Paramedian: The LDH arises slightly displaced from the midline, to the right or left, but still protrudes into the spinal canal.

- Foraminal: The LDH arises in the intervertebral foramen (the space through which the nerve root exits the spine).
- Extraforaminal: The LDH arises beyond the foramen, more laterally in relation to the spinal canal.

Figure 2.3 shows the location of the LDH according to its topography.

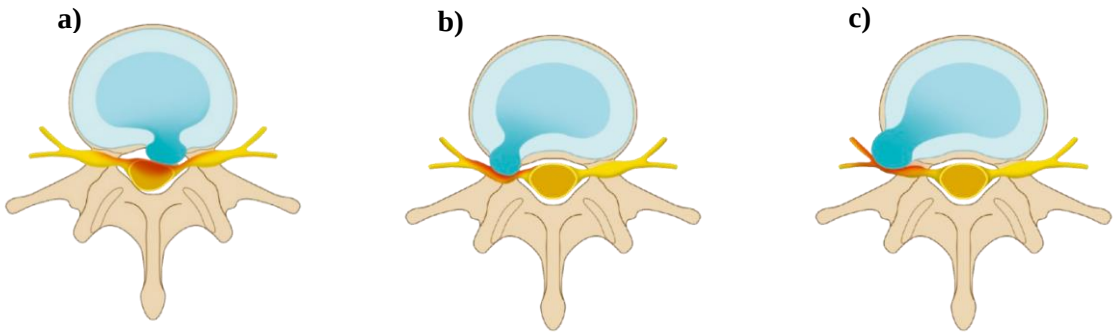

Figure 2.3 – Types of LDH topography: a) Median/Paramedian, b) Foraminal and c) Extraforaminal [23].

Finally, the last qualitative parameter that needs to be evaluated in MRI is the Pfirrmann Grade, which is a classification system used to assess the degree of degeneration of the IVDs in the spine. This classification is divided into 5 grades, ranging from I to V, where Grade I indicates a healthy IVD and Grade V represents a highly degenerated IVD. The classification is based on four main criteria such as: IVD structure, distinction between the NP and the AF, signal intensity on T2 and IVD height. Table 2.1 presents the various grades according to the different criteria, while Figure 2.4 illustrates the different degrees of IVD degeneration classification [24].

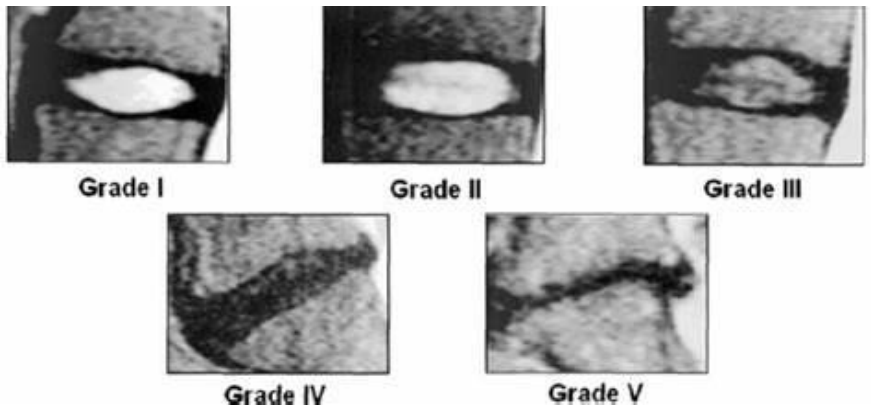

Figure 2.4 – Illustrative Pfirrmann's classification system [25].

Table 2.1 – Pfirrmann's classification of IVD degeneration [24].

Grade	IVD structure	Distinction between the NP and AF	Signal intensity	IVD height
I	Homogeneous, bright white	Clear	Hyperintense, isointense to cerebrospinal fluid	Normal
II	Inhomogeneous with or without horizontal bands	Clear	Hyperintense, isointense to cerebrospinal fluid	Normal
III	Inhomogeneous, grey	Not clear	Intermediate	Normal to slightly decreased
IV	Inhomogeneous, grey to black	Loss	Intermediate and isointense	Normal to moderately decreased
V	Inhomogeneous, black	Loss	Hypointense	Collapsed IVD space

2.3.2 Conservative and surgical treatment

Conservative treatment includes physiotherapy with the aim of reduce pain and improve functional capacity. The aim of conservative treatment is to relieve pain and stimulate neurological recovery, so the patients can quickly return their daily and occupational activities. The patients who benefit most from this treatment are young patients with small LDHs, minimal IVD degeneration and minor neurological function loss. When patients have a severe sciatica episode, they are incapacitated, treatment should aim to gradually reduce pain, increase physical activity levels and avoid absolute rest. Non-steroidal anti-inflammatory drugs should be administered to meet the pathophysiological needs. An alternative to assist conservative treatment is blocking the affected root with anaesthetics and corticosteroids, which act directly on the nerve root by decreasing its inflammatory response [3].

The aim of surgical treatment is to decompress the nerve roots. This treatment is performed when there is a sciatica that does not respond to conservative treatment for at least 6 weeks, motor deficit greater than grade 3 or nerve root pain associated with foraminal bone stenosis. The surgical techniques used by most surgeons are traditional discectomy and microdiscectomy, with the latter being the preferred technique both in the short term (operation duration, bleeding, symptom relief and complication rate) and in the long term (return to daily activities and work). Surgical treatment is favourable as it enables an early return to work [3].

The choice of the treatment group for each patient is made based on the presence of a positive "Straight Leg Raise Test", and a combination of clinical data regarding the type, intensity and duration of symptoms, as well as the diagnosis from imaging studies, specifically MRI or CT scans. The "Straight Leg Raise Test" is a neurological physical examination used

to assess the presence of nerve compression in the lumbar spine. During this test, the physician raises the patient´s extended leg, while the patient is lying on their back, in order to change the angle of lumbar lordosis and reduce the area of the central canal and foramen. If the patient feels extreme pain when the leg is raised with less than 30 degrees, the test is considered positive. That said, if the patient has been experiencing symptoms for several months and the diagnostic exam reveals a LDH significantly compressing a nerve root, the patient will be placed in the surgical treatment group. Conversely, if the patient feels pain during the leg raise, but the duration of symptoms is low, regardless of having a large LDH on the exam, the patient will be placed in the conservative treatment group [26].

2.4 Diagnostic and evaluation methods

2.4.1 Imaging of the lumbar spine

Medical imaging exams are often proposed to patients with LBP and/or leg pain to assess nerve root compression caused by LDH, with CT and MRI being the gold standard [27].

Between the two, MRI is the primary choice, given its relatively high sensitivity (75%) [27]. Although MRI is an excellent exam for characterising degenerative IVD disease, it significantly underestimates nerve root compression caused by degenerative changes in the lateral recess [28]. In addition, MRI and CT studies provide a static dataset and often underestimate the anatomical changes that occur in LDH because they are performed in the supine position, a relatively unloaded position [29].

Sciatica symptoms usually develop when the patient is standing and walking, reflecting an inherent biomechanical component of the disease. Therefore, test should be carried out with the patient standing, such as Standing X-ray and Functional X-ray to obtain outputs with the patient in supine and standing position, for later comparison [29].

Additionally, the poor correlation that has been observed between clinical and MRI findings in patients with LDH, and the presence of typical changes on MRI of patients with LDH in asymptomatic individuals, justifies the combination of clinical and MRI findings to accurately diagnose and treat patients [29].

2.4.1.1 CT

CT is a non-invasive medical imaging technique used to visualize organs and tissues such as the heart, liver, lungs, skull and spine, among others. In the lumbar spine, this technique is used for the detailed evaluation of bone structures and is highly sensitive in detecting fractures. This diagnostic method is based on exposing the patient to X-rays (ionizing radiation) to acquire a volume of data from the body, which is processed by a computer to create cross-sectional images of the inside of the body. During the exam, the patient remains in a supine position. Occasionally, a contrast agent is administered orally or intravenously to improve the visibility of specific tissues or blood vessels, facilitating a more accurate diagnosis. CT images are represented in greyscale and offer excellent spatial resolution, particularly in visualizing bone structures and detecting lesions with different densities [30].

2.4.1.2 MRI

MRI is an exam that uses technology based on radiofrequency waves in a strong magnetic field to obtain body images in various planes. First, the patient lies down in the supine position to begin the exam. The magnetic field aligns the hydrogen protons in the body, which have a magnetic moment due to their spin. Then, radiofrequency pulses are applied to temporarily misalign these protons. After the radiofrequency pulses are switched off, the hydrogen protons return to their equilibrium state, realigning with the magnetic field. During this relaxation time, the protons emit radiofrequency signals that are detected by an antenna [31], [32].

Relaxation occurs in two phases: longitudinal relaxation (associated with T1 weighting), which consists of the time needed for the protons to realign with the central magnetic field, and transverse relaxation (associated with T2 weighting), which corresponds to the time taken for the protons to lose coherence with each other in the plane perpendicular to the field. Finally, the computer processes these signals using the Fourier Transform, converting them into 3D images of the inside of the body [31], [32].

T1 and T2 weightings refer to different ways of highlighting tissues based on spin-lattice (T1) and spin-spin (T2) relaxation times. In T1-weighted images, fat-rich tissues appear brighter, while in T2-weighted images, water-rich tissues (such as IVDs and cerebrospinal

fluid) appear brighter. The choice of weighting depends on the type of analysis or diagnosis that is intended [32].

Unlike CT, MRI does not use ionizing radiation, making it a safer imaging modality in terms of radiation exposure. MRI allows for a more accurate diagnosis in many cases, especially in the evaluation of soft tissues, joints and the central nervous system, as it offers excellent contrast resolution for these tissues. MRI has been considered the most appropriate diagnostic modality for assessing spinal pathologies, as it allows for the visualization of the entire spine and differentiation of individual structures such as vertebral bodies, IVDs, the spinal canal, ligaments, nerve roots and the spinal cord. This makes it superior to CT in the detailed visualization of body parts such as the brain, muscles, joints and internal organs. However, the main disadvantage of MRI is the exam duration, which can be significantly longer than CT, which can be a limitation in certain clinical situations, and it's worse than CT for bone evaluation [31].

2.4.1.3 Standing X-ray

Standing X-ray is a non-invasive medical imaging technique that can visualize bone structures, joints and dense tissues such as the lungs and heart. The technique is widely used to detect bone fractures, infections, tumours and other medical conditions [33].

The Standing X-ray technique involves exposing a part of the body to ionizing radiation. During the exam, a generator emits X-ray beams that pass through the body and are captured by a detector or film. Different body tissues absorb X-rays in different ways. For example, bones, being denser, absorb more radiation and appear brighter on the image, while soft tissues, such as muscles and organs, allow more X-ray beams to pass through, appearing darker on the resulting image. Despite the benefits, the use of X-ray requires precautions due to radiation exposure. Unlike CT and MRI, to analyse the lumbar spine, the patient is positioned standing up [33].

Images generated by Standing X-ray are generally two-dimensional (2D), providing a flat view of internal structures. However, CT is an advanced technique based on X-rays that generates 3D images by combining multiple 2D images from different angles [33].

2.4.1.4 Functional X-ray

Functional X-ray is a non-invasive medical imaging technique that differs from Standing X-ray as it allows for the analysis of dynamic body functions, such as joint movement and spinal instability. With this type of imaging, doctors can observe in real time the functioning of various parts of the body in motion, as this method involves capturing a series of images in rapid sequence, creating a kind of real-time "video" of internal structures in motion [34], [35].

As Standing X-ray, Functional X-ray use ionizing radiation, which can penetrate the body and create images of internal structures. In addition, the images generated by Functional X-ray are typically 2D. The advantage of this technique lies in the ability to capture moving images, providing a dynamic visualization in real time [34], [35].

At the lumbar spine level, Functional X-ray are used to detect vertebral instabilities, dynamic spondylolisthesis and hypermobility/hypomobility, in order to help with surgical decisions. This is done by performing flexion and extension movements of the spine, allowing precise assessment of these conditions during movement [34], [35].

2.4.2 Gait analysis

The gait cycle is evaluated as a complement to the diagnosis of LDH based on medical imaging, providing additional functional information [36]. In healthy patients, the gait cycle is characterised by symmetry, balance and fluid movement, with a well-coordinated pattern between the two phases (stance and swing phase), allowing for regular and uniform locomotion [36].

However, LDH patients have difficulty walking and usually walk more slowly than healthy patients, resulting in gait discoordination [37]. Degeneration of IVD, in addition to LBP, can cause changes in spatio-temporal characteristics (speed or step length), kinematics (joint/segment movement or coordination between joints/segments), kinetics (joint forces and torques), electromyography characteristics (amplitude and timing of muscle activation) with gait instability associated with LBP [4], [5].

Gait tests show that LDH patients adopt compensatory patterns to reduce pain and avoid overload, such as shorter steps, reduced pelvic rotation and decreased knee flexion. These

changes can lead to an asymmetrical and unstable gait, with one side bearing more weight. Muscle weakness can cause foot dragging and reduced step height during swing phase, while LBP limits hip extension, disrupting movement fluidity [5], [38].

2.5 Image segmentation and modelling

Understanding bone anatomy is extremely important for spine doctors. One way to study this branch of anatomy in order to train surgical technique is through cadavers, whose availability is limited. Therefore, there is an alternative way of using images and models reconstructed in 3D for the same purpose. These 3D models are reconstructed using medical imaging methods, such as MRI and CT, and have the advantage of being reusable and can be constructed whenever needed [8].

There are numerous software programs for reconstructing 3D models, with step-by-step protocols to guide the surgeons in performing 3D reconstructions in the office. Nevertheless, there is no consensus on the ideal method for reconstructing 3D models of the lumbar spine from MRI and CT images, which can reproduce a very realistic 3D model quickly, leading to discrepant outputs between surgeons [8].

Spinal column segmentation for clinical purposes is still typically performed manually, selecting the vertebral bone area on sagittal, coronal and axial slices that correspond to the region of interest, from which the 3D reconstructions is made. In non-automated software, it is necessary to manually select the area of the structure under analysis in multiple sections across the different planes. In contrast, automated software can segment the vertebrae by analysing texture, pixel intensity and contrast between the bone and surrounding structures. Some software allows for visual refinement, such as smoothing irregularities, to make the resulting structure as close as possible to the patient´s lumbar spine. However, in certain software, this option is unavailable, requiring the use of additional software for 3D model editing and visual enhancement. Depending on the need, the 3D models can be printed on 3D printers, allowing the surgeon to practise or plan the surgery without the need to use a cadaver [8].

Although the approach to reconstruct 3D models seems to be a simple and useful method using automatic segmentation software, the process is time-consuming, which explains why it is still not commonly used in clinical practice. Therefore, is necessary to have a software that

could load the patient's MRI/CT images and automatically segment the structures under analysis in the shortest possible time [8].

Finally, the reconstructed 3D models can be used for additional finite element analysis to simulate how the lumbar spine behaves under various physical conditions, such as forces, stresses and deformations, etc. When the finite element method is applied to a 3D model of the lumbar spine, detailed information about the mechanical and structural behaviour of the spine under different scenarios is provided [8].

Matos work in 2021 [39] aimed to develop a method for the automatic 3D localisation and segmentation of lumbar IVD, from T2-weighted MRI images. These models were used to assist in constructing finite element models of the lumbar spine based on real cases, providing accurate and personalized information about the shape of the patient's IVDs. The segmentation method was developed from a pre-existing method in the literature for performing 2D segmentations in the sagittal plane, and it was partially modified based on statistical models created to estimate the width of the IVDs and the shape of the vertebral bodies, then adapted for 3D use, utilizing 3D Slicer and ITK-Snap software. The proposed method allowed for the 3D segmentation of IVD with a Dice Coefficient (which measures the proportion of correctly identified points) of 87.0 ± 3.7% in a time of 6-7 seconds. Currently, the use of 3D data in clinical practice is rare due to a lack of tools that enable its rapid availability and interpretation by professionals, with 2D slices being preferred to approximate the spatial morphology of the spine. In this way, Matos demonstrated that the method used allows for the generation of 3D models relatively quickly and accurately, providing an alternative to the use of 2D data and its inherent limitations. Although the accuracy of the method is not high enough to allow for fully automatic segmentation, it still significantly reduces the amount of manual work required for 3D segmentation, opening possibilities for its use in 3D finite element modelling and simulation.

Furthermore, a method was developed based on the analysis of intensity and the NP/AF ratio of the IVD, which allowed for a binary classification of the IVDs degenerative state. This method enabled the separate segmentation of the two main structures of the IVD – the AF and the NP – (Pfirrman Grade between I and II) and automatically detected cases where the degeneration did not allow for this distinction (Pfirrman Grade between III and V) through image processing. This method demonstrated an effectiveness of approximately 96% [39].

Pernas work in 2023 [40] focused on the computational analysis of 3D models of spines with adolescent idiopathic scoliosis, where three spines from patients with different scoliosis classifications (both in Cobb angle and curvature type) were analysed and compared with two spines from patients without pathologies. The Cobb angle is the characterisation method used in diagnosis; however, its individual use is insufficient for understanding and planning treatment. Thus, vertebrae were quantified through the development of a methodology based on extraction of centroids for each vertebra (semi-automatic method using MeshLab) and their intersection with planes that define the position of the respective axes for each component (manual method using 3D Slicer). The parameters analysed in the study included the Cobb angle (2D and 3D), angular deviation, rotation occurring within the spine itself, and rotation of each vertebra individually. The combination of these parameters allowed for the study of the position and variation of each vertebra, assisting in the computational process.

Regarding the exams necessary for the diagnosis and classification of scoliosis, X-ray and MRI are the most commonly performed tests; however, CT scans can provide a more comprehensive and accurate assessment. The comparative evaluation between 2D and 3D, as well as the CT method against conventionally performed examinations, showed significant differences, enhancing the quality or qualification when using the 3D CT methodology. Thus, it was demonstrated that the study conducted in 3D is more viable, as the 2D assessment showed low values due to a lack of information from one of the planes [40].

Wang et al. in 2022 [41] developed a method for IVD recognition and disease classification to improve the accuracy and efficiency of LDH diagnosis using MRI with T2-weighted and machine learning techniques. The method consisted of 3 steps: image preprocessing, target segmentation and symptom classification. Preprocessing was carried out using noise reduction methods and interference removal methods in blurred images. The segmentation of the vertebrae was achieved through a multi-thresholding method and a greyscale threshold binarization method. Subsequently, a contour screening was performed based on area and shape characteristics. Following this, the positioning of the vertebrae was verified to determine whether the IVD is herniated or not. However, the S1 vertebra is different from the lumbar vertebrae, and thus contour pole was used to identify four points of the vertebra in order to reduce incorrect segmentation of the S1 vertebra. To complete the segmentation, the IVDs were segmented, distinguishing the NP from the AF, which resulted in better segmentation compared to the vertebrae. The final stage, corresponding to the LDH diagnosis, utilised 3 indicators:

diagnosis with protrusion distance, diagnosis with the average grey scale and diagnosis with spinal canal recognition.

A preliminary diagnosis can be made by the identification and localisation of vertebrae and IVDs, but this diagnosis is not uniform criteria and not suitable for automatic computerized diagnosis. Thus, a classification method based on five judgment indexes has been proposed – protrusion distance, protrusion area, protrusion length ratio, protrusion area ratio and average grey level – which improves the stability of the disease diagnosis [41].

The experimental results showed that the classification accuracy of the validation set, and test set reached 91% and 92%, respectively, which demonstrates the effectiveness of the method. Thus, this system leverages and structural and morphological characteristics of MRI images to automated the diagnosis of LDHs, significantly increasing both speed and reliability. Automated processes offer potential improvements in clinical diagnosis by reducing human error and enhancing consistency in the interpretation of MRI examinations for LDH [41].

Van der Graaf et al. in 2024 [42] presented a lumbar spine MRI dataset, with the aim of automatically and accurately segmenting structures such as vertebrae, IVDs and the spinal canal, using the 3D Slicer software. The dataset consisted of 447 sagittal T1 and T2 series of images from 218 patients with a history of LBP, collected from 4 different hospitals. To develop a robust benchmark, the authors implemented an iterative annotation approach. Initially, a deep learning segmentation algorithm was trained on a small sample of the dataset, producing semi-automatic results that were manually reviewed and corrected. These corrections were integrated into the training algorithm, progressively increasing its accuracy.

This study was of high importance as it compares segmentation algorithms, especially nnU-net, one of the most efficient models in biomedical segmentation. In addition, the article encourages the scientific community to develop and test new algorithms, promoting technological and clinical advances in image segmentation in the lumbar spine. This has the potential to significantly improve diagnostic quality and inform surgical planning for spinal pathologies [42].

3. Methodology

3.1 Type of study

An observational cross-sectional study was conducted with a sample of 10 patients.

3.2 Sample

The inclusion criteria described in the protocol were as follows: (1) age between 18 and 75 years; (2) established diagnosis of LDH based on clinical and imaging criteria (prolapse, protrusion, extrusion or sequestration); (3) radicular pain with evidence of nerve-root irritation with a positive nerve-root tension sign and (4) ability to provide consent.

Conversely, the exclusion criteria were as follows: (1) previous spine surgery; (2) cauda-equina syndrome; (3) neurological disease that might interfere with gait; (4) known orthopaedic conditions that significantly disrupt gait, as per investigator judgement; (5) severe comorbidity; (6) vertebral fractures; (7) spine infection or tumour; (8) pregnancy; (9) dementia or any other form of cognitive impairment; (10) inability to provide informed consent and (11) spondylolisthesis and/or spinal instability.

3.3 Study procedures

The Study Protocol and all relevant documentation was submitted for approval by the Research Board and Ethics Committees of Grupo Luz Saúde. The approval of these documents ensures compliance with ethical principles and applicable international, community and national legislation, including the Helsinki Declaration and the European Charter of Fundamental Rights.

After ethics approval, patients with LDH were recruited from the outpatient clinic of the Neurosurgical Department of HLS between April and September 2024. The informed consent document given to the patient contained a detailed description of the study, as well as information about its duration, risks, confidentiality and the participant's rights. After checking for eligibility and obtaining written consent, all participants were assigned a study identification number (example: HLS.053).

3.3.1 Clinical assessment

The selection of the initial diagnostic exam in this study reflects a bias linked to the Neurosurgical Centre setting, where patients are referred for severe pain or prolonged symptoms duration, for the purpose of determining a more complex treatment, such as surgical intervention. In these situations, the neurosurgeon typically chooses an MRI over a CT scan as the initial image exam for the diagnosis, due to its specificity in visualizing the IVDs.

After performing a diagnostic exam (MRI or CT), a neurosurgeon defines the treatment protocol according to his judgement and standard of care, based on the presence, intensity and duration of LBP and radicular pain, as well as confirmation of LDH through imaging exams.

Patients with LDH and mild symptoms are included in the conservative treatment group, while patients with moderate to severe symptoms of some duration are included in the surgical treatment group.

In the same consultation, gait analysis was performed using a 3D full-body kinematics analysis system based on inertial sensors.

3.3.2 Data collection

The data was recorded in a database (DB) developed exclusively for the study, which included: (1) social and demographic data (age and sex); (2) standardized clinical evaluation (height and weight); (3) treatment group; (4) Numerical Pain Rating Scale (NPRS) for pain (axial and radicular pain) and (5) Oswestry Disability Index (ODI) for the impact of pain in function. All the questionnaires are validated for the Portuguese population.

The NPRS is a numerical scale used to measure pain intensity, serving as a quick estimate of the patient's perception of pain. Patients rate their pain on a scale from 0 to 10, where 0 means "no pain" and 10 means "the worst pain possible". The NPRS is used to assess different types of pain, such as axial and radicular pain, in their basal and peak states. Axial pain refers to pain centred on or around the spine, without radiating to other parts of the body. Radicular pain radiates along the lower limb, often caused by compression or irritation of a nerve root. The basal state of pain refers to the pain the patient feels most of the time, while the peak state refers to the maximum intensity of pain the patient experiences during flare-up or crises [43].

The ODI is a questionnaire used to evaluate functional disability related to LBP, measuring how pain affects the patient's daily activities. This questionnaire is divided into 10 sections, each addresses a different aspect of daily life, such as pain intensity, personal care, weightlifting, walking, sitting, standing, sleeping, sexual life, social life and travelling. Each section is scored from 0 to 5, giving a maximum score of 50. This score is converted into a percentage by multiplying it by 2. The scores are then divided into different levels of severity: 0-20 minimal disability; 21-40 moderate disability; 41-60 severe disability; 61-80 crippling back pain and 81-100 patients with extreme symptoms [44].

3.3.3 Image assessment

The diagnosis of LDH for all patients, except in HLS.063, was based on MRI outputs, which were collected by a GE 3T MRI, model Signa Architect AIR. The MRI exam of patient HLS.063 was carried out at another clinic/hospital. During the MRI, patients were positioned in the supine position. In addition to the MRI, it was also checked whether each patient had a CT scan, a Standing X-ray and a Functional X-ray, in order to compare all medical imaging modalities. CT images were collected using by a CANON model Aquilion Prime 64-slice CT scanner and the examination was performed with the patient in the supine position. Standing and Functional X-ray images were collected using by a RANON model RADREX machine, with the patient in a standing position. In the case of the Standing X-ray, the patient is in a neutral standing position and for Functional X-ray, the patient performs a flexion and extension movement.

After verifying the exams each patient had, quantitative and qualitative parameters were extracted from MRI image analysis, which were considered relevant to the study of LDH and potentially related to the clinic presentation. Subsequently, the same parameters were checked for the remaining medical imaging modalities, and all were extracted using the Carestream Vue Motion and Carestream Client software (Onex Corporation, EUA). These parameters were selected based on literature review [27], [29] and the opinions of neurosurgeons, radiologists and imaging technicians at HLS. The Carestream Client software, unlike Carestream Vue Motion, has area measurement functionalities, however, for height and distance measurements, Carestream Vue Motion provides greater precision, as the outputs are displayed with two decimal places. Thus, the Carestream Client software was only used for area measurements,

while the other parameters were obtained with Carestream Vue Motion. Table 3.1 shows the qualitative and quantitative parameters taken from each medical imaging modality. The quantitative parameters extracted, along with the plane, slice, measurement units and measurement methods are presented and illustrated in Appendix 1.

Table 3.1 – Parameters by medical imaging modality.

Parameters	**MRI**	**CT**	**Standing X-ray**	**Functional X-ray**
LDH level	x			
LDH type	x			
LDH topography	x			
LDH location	x			
Pfirmann grade	x			
Nerve root compression	x			
IVD height (Sagittal)	x	x	x	x
IVD height (Coronal)	x	x	x	
Vertebra height (Sagittal)	x	x	x	x
Vertebra height (Coronal)	x	x	x	
IVD length	x	x		
Intervertebral angle (Sagittal)	x	x	x	x
Intervertebral angle (Coronal)	x	x		
Lumbar lordosis angle	x	x	x	x
Anterior-posterior canal diameter at vertebrae level	x	x		
Anterior-posterior canal diameter at IVD level	x	x		
Largest anterior-posterior projection of the LDH	x	x		
Central signal	x			
Herniation signal	x			
Canal area without LDH	x	x		
Foramen area (left and right)	x	x	x	x
Nerve root area (left and right)	x	x		
Useful foramen area (left and right)	x	x		
Largest foramen diameter (left and right)	x	x	x	x
Largest nerve root diameter (left and right)	x	x		

In order to provide guidance over the quantitative parameters evaluated in this study, the following details need to be taken into consideration: i) in CT scans, since the IVD are not always clearly visible, the parameters “central signal” and “herniation signal” are not extracted; ii) in Standing and Functional X-ray, the IVD is not visible and therefore the “IVD length”, “central signal” and “herniation signal” are not measured; iii) the coronal plane in Standing X-ray does not allow for the measurement of the “intervertebral angle”, so this parameter was excluded; iv) it is also not possible to visualize the intervertebral canal, so the “anterior-posterior canal diameter at vertebral and IVD levels” were not included; v) as X-rays techniques do not present the axial plane, it was not possible to measure the “largest anterior-posterior projection of the LDH” and the “canal area without LDH”; vi) it is also not possible to visualize the nerve roots within the foramen, so the parameters “nerve root area (left and right)” and

“largest nerve root diameter (left and right)” were not extracted; vii) in both X-rays techniques, the central heights of the IVDs and vertebrae were not measured since 2D images lose information compared to 3D images and there is a possibility of overlap of information in 2D images; viii) lastly, in both X-rays, it is not possible to distinguish between left and right foramen, since they show a profile view, so only the value of the visualized foramen is presented, i.e., the only difference between the parameters measured in Standing X-ray and Functional X-ray is that in the latter, the coronal plane is not visualized.

Analysing the parameters in Table 3.1 and Appendix 1, it is important to highlight that the images included in the examples are only from MRI exams; they belong to the patients analysed in this study and the measurements were taken by the author of the study. Additionally, it is important to note that the lines corresponding to the heights of the IVDs and vertebrae did not always have the same slope, as the inclination of the spine varies from level to level in each patient. Not all exams included the coronal plane (MRI and Standing X-ray), since they were possibly not performed using the same protocol, which will interfere with the reproducibility of the outputs. In certain MRI exams, the coronal plane was not present, but there was a “Plane Localizer” that shows some images in the coronal plane. The Plane Localizer only presents one image with all the vertebrae and as such, this image may not correspond to the correct mid-plane. Furthermore, the image quality of the Plane Localizer is very poor and as a result, the measurements can be quite different between different measurements. In terms of measurements, for L5-S1 level, it is not possible to determine the IVD height in the coronal plane or measure the “intervertebral angle” because the S1 vertebrae is “displaced” relative to the other lumbar vertebrae and therefore, the intervertebral angle would not be correct. The “lumbar lordosis angle” was measured from the superior endplate of L1 to the superior endplate of S1, as this parameter must be assessed by considering the same number of segments, that is, 5 vertebrae and 5 IVDs.

Subsequently, the parameters described in Table 3.2 were extracted 3 times, with intervals of one week, to obtain a reliable average of the outputs, while avoiding the effect of bias/ “adaptation” in the measurements. The parameters listed in the table below were selected because they are believed to best characterise each imaging technique, according to the opinion of the doctors and professionals at HLS and the authors of this paper. Thus, this methodology will result in intra-observer variability, but not inter-observer variability.

Table 3.2 – Parameters measured 3 times according to medical imaging modality.

Parameters measured 3 times	MRI	CT	Standing X-ray	Functional X-ray
IVD height (Sagittal)	x	x	x	x
IVD height (Coronal)	x	x	x	
Vertebral height (Sagittal)	x	x	x	x
Vertebral height (Coronal)	x	x	x	
IVD length	x	x	x	
Intervertebral angle (Sagittal)	x	x	x	x
Intervertebral angle (Coronal)	x	x		
Lumbar lordosis angle	x	x	x	x
Central signal	x			
Herniation signal	x			
Foramen area			x	x
Largest foramen diameter			x	x

After obtaining the average of the 3 measurements for each parameter, of each patient and in each medical imaging modality, the outputs were compared between imaging modalities. The analyses performed were as follows: i) MRI versus CT; ii) MRI versus Standing X-ray and iii) MRI versus Functional X-ray. The purpose of these combinations of exams is to evaluate the difference between patient positions during the exams and the variability of the outputs. To analyse the outputs of these exams combinations, Equation 3.1 was applied for each parameter, which is based on a percentage deviation analysis between 2 imaging techniques. The formula shown below demonstrates an example with parameter 1 between MRI and CT, where P1 (MRI) represents parameter 1 of MRI and P1 (CT) represents parameter 1 of CT.

$$\frac{P1\ (MRI) - P1\ (CT)}{P1\ (MRI)} \times 100 \tag{3.1}$$

A positive value of the percentage deviation means that the MRI measurement is higher than in the other imaging modality (or vice-versa). Using an example from the DB developed and considering the parameter "IVD height L1-L2 (anterior side)", in the sagittal plane, the average parameter in MRI was 7.24 mm and in CT it was 4.25 mm. Applying equation 3.1, the following expression was obtained:

$$\frac{7{,}24 - 4{,}25}{7{,}24} \times 100 = 41{,}30\%$$

Figure 3.1 shows the height of the IVD (anterior, central and posterior) at the L2-L3, L3-L4 and L4-L5 levels in a) MRI and b) CT, of patient HLS.055. It can thus be seen that the measurements are different between the 2 imaging modalities in the same individual and, as such, this difference is verified in % using equation 3.1. The measurements shown refer to 1 of the 3 measurements taken for each imaging modality on the same individual.

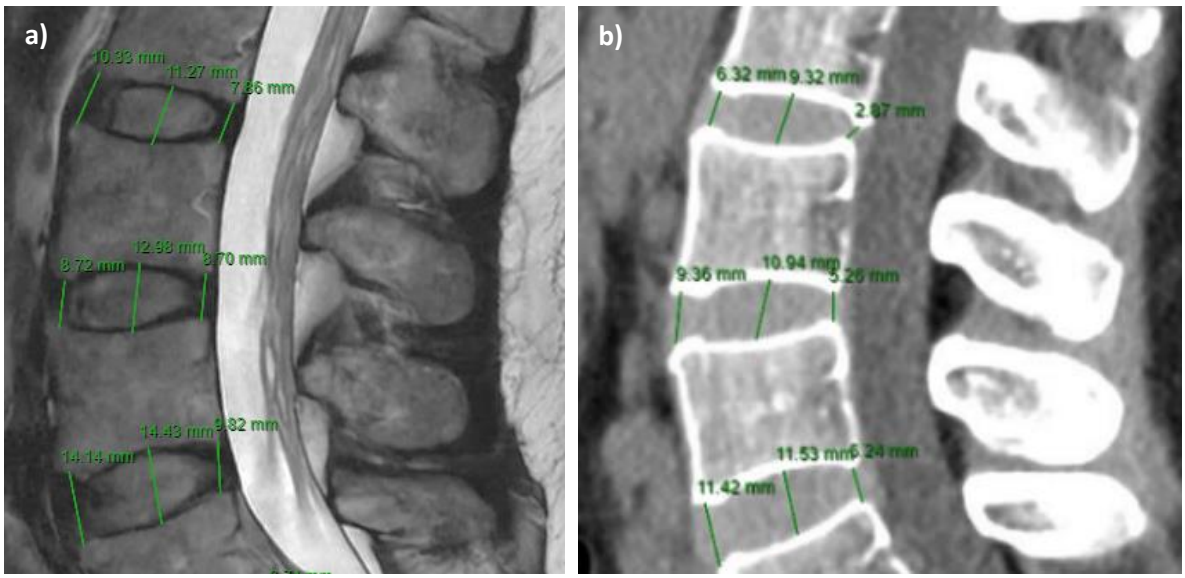

Figure 3.1 – Comparison of "IVD height" parameter in different imaging modalities a) MRI and b) CT, of patient HLS.055.

3.3.4 Computational modelling

From CT images, 3D computational models of the 5 lumbar vertebrae and the first sacral vertebra were developed, using ITK-SNAP® (University of Pennsylvania, EUA), which is an open-source tool for semi-automatic segmentation of medical images. Subsequently, the generated models were imported into MeshLab® (an open-source 3D modelling software, ISTI-CNR, Italy) to be improved. This involved removing unnecessary material, repairing holes and imperfections and enhancing the surfaces of the models.

Once this process was completed, according to the medical imaging modality used (CT) and based on the parameters in Table 3.2, the following parameters were taken: IVD height (sagittal and coronal plane), vertebral height (sagittal and coronal plane), intervertebral angle (sagittal and coronal plane) and lumbar lordosis angle. As previously mentioned, each extracted parameter was measured 3 times and the average of these 3 values per parameter was calculated

for each 3D model. Finally, the average value of each parameter, corresponding to each 3D model, was compared with the average value of each parameter, corresponding to the MRI measurements, using equation 3.1, forming the MRI versus 3D models combination.

Figure 3.2 shows an image of the 3D model of each patient in the sagittal plane.

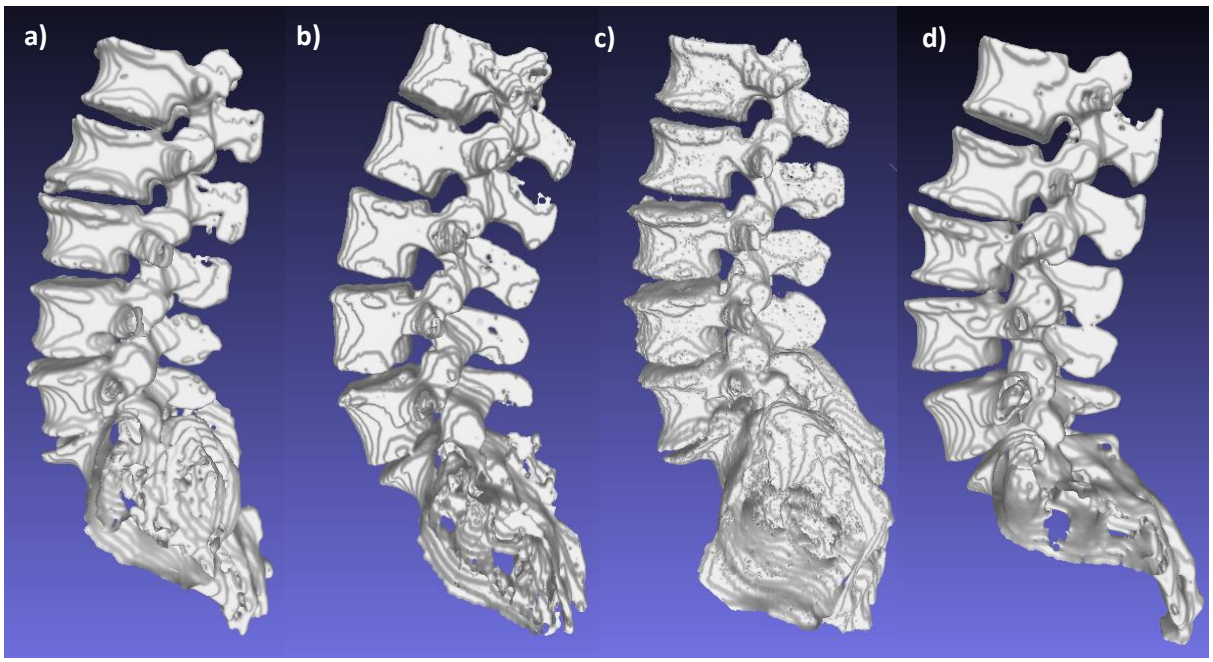

Figure 3.2 – 3D models of patients a) HLS.053, b) HLS.055, c) HLS.056 and d) HLS.067.

3.3.5 Database

An EXCEL DB was created, consisting of: clinical data such as age, sex, height, weight, BMI (Body Mass Index), treatment group, dominant symptoms, symptomatic levels, LDH level, symptom laterality, NPRS and ODI (Appendix 2); parameters described in Table 3.1; parameters described in Table 3.2, measured 3 times for each imaging modality and for the 3 models developed; the average of the 3 measurements for each patient, for each parameter (2D and 3D) and for each imaging modality, as well as the average of each parameter for each imaging technique (Appendices 3, 4, 5 and 6); and the comparison of the various imaging modalities based on the different combinations, using equation 3.1 described above.

Table 3.3 presents the medical imaging exams for each patient. It can be confirmed that all patients in the study had the MRI exam, as it is the primary diagnostic exam. Only 4 patients (HLS.053, HLS.055, HLS.056 and HLS.067) presented CT, and as a result, only these patients

had a 3D model of the lumbar spine. On the other hand, there were 9 patients with Standing X-ray and 8 patients with Functional X-ray.

Table 3.3 – Exams that each patient had.

HLS	MRI	CT	Standing X-Ray	Functional X-Ray
HLS.053	x	x	x	x
HLS.055	x	x	x	x
HLS.056	x	x	x	x
HLS.062	x		x	x
HLS.063	x			
HLS.064	x		x	x
HLS.067	x	x	x	x
HLS.070	x		x	
HLS.072	x		x	x
HLS.075	x		x	x

The 10 patients were divided into 2 groups for the outputs analysis. Group 1 consists of the 8 patients who have Functional X-ray, as well as MRI and Standing X-ray. Group 2 consists of the 4 patients who have all the exams.

To analyse the outputs, different data analysis methods were used, such as:

1) Relation between NPRS/ODI and age, sex, BMI and LDH area;
2) Comparison of IVD height (anterior and posterior) between patients with LDH and healthy patients, and its relation with NPRS and ODI (the IVD height measurements in healthy patients used, were taken from [45]);
3) Analysis of the average parameters in each imaging modality;
4) Analysis of the percentage deviations of each parameter (IVD height, vertebral height, intervertebral angle and lumbar lordosis angle) between different medical imaging modalities.

Analysis 1), and 2) were conducted individually with the 10 patients. Analysis 3) was performed using the average of each parameter by imaging technique, according to the total number of patients that each technique includes. Finally, analysis 4) was conducted for each group of patients defined above.

The sample consisted of 6 women and 4 men, aged between 28 and 75 years. These patients had an average of 53.80 ± 12.19 years, with height of 1.69 ± 0.07 m, an average weight of 87.30 ± 24.29 kg and an average BMI of 30.00 ± 6.46 kg/m^2.

Table 3.4 shows the BMI classification according to the different weight-for-height ranges, as described in the literature [46]. Table 3.5 shows the number of patients in the study according to their BMI.

Table 3.4 – BMI classification according to the literature [45].

BMI Classification	
Underweight	< 18,50 kg/m^2
Normal Weight	18,50 – 24,90 kg/m^2
Overweight	25 – 29,90 kg/m^2
Obesity Grade I	30 – 34,90 kg/m^2
Obesity Grade II	35 – 39,90 kg/m^2
Obesity Grade III	> 40 kg/m^2

Table 3.5 – Number of patients according to their BMI.

BMI Classification	
Underweight	0
Normal Weight	2
Overweight	4
Obesity Grade I	1
Obesity Grade II	3
Obesity Grade III	0

Table 3.6 shows some clinical parameters taken from the patients in the study. The same patient can have more than one affected IVD and, as such, were studied 14 different affected IVDs in 4 different levels. The patients could belong to the conservative treatment or surgical treatment group. In terms of pain laterality, patients could have left, right and bilateral symptoms.

Table 3.6 – Some clinical parameters taken from study patients.

Clinical parameters	
Levels of IVDs affected	L2-L3: 1 L3-L4: 3 L4-L5: 4 L5-S1: 6
Treatment Groups	Conservative: 3 patients Surgical: 7 patients
Pain Laterality	Left: 5 patients Right: 4 patients Bilateral: 1 patient

4. Results and Discussion

This study aimed to correlate the clinical characteristics, the quantitative and qualitative parameters of the various imaging modalities and the quantitative parameters of 3D models, in patients with LDH manifested as acute sciatica.

In Appendix 2, the socio-demographic data collected in this study is displayed, as well as information about each patient's LDH, collected by the neurosurgeon during baseline clinical evaluation. In terms of sex, this sample revealed that LDH is slightly more prevalent in women than men, however, this condition manifests slightly more in males than females [3]. Regarding age, LDH appears mainly between the ages of 40 and 50, so the average age of the study sample (53.80 ± 12.19 years) is not too far off. According to the literature, overweight and obese individuals are more likely to develop LDH, as a high BMI exerts greater pressure on the spine, particularly in the lumbar region, which can accelerate the degeneration of the IVDs [47]. In addition, excess weight can cause malalignment of the lumbar spine and increase the load on the IVDs. Considering the study sample, the average BMI is within the overweight range, which supports the evidence of LDH and BMI association.

4.1 Initial analysis

The qualitative parameters were estimated from MRI scans for each LDH in each patient and then validated by Dr. Nuno Cristino. Table 4.1 shows all the qualitative parameters for each patient in the study.

Table 4.1 – Qualitative parameters taken from MRI scans for each LDH in each patient.

HLS	LDH level	LDH type	LDH topography	LDH location	Pfirrmann Grade	Nerve root compression
HLS.053	L4-L5	Protrusion	Paramedian/Foraminal	Descending	III	L4 and L5 (left)
HLS.055	L5-S1	Extrusion	Paramedian	Descending	IV	S1 (left)
HLS.056	L4-L5	Prolapse	Median/Paramedian	IVD level	III	L4 and L5 (left and right)
	L5-S1	Protrusion	Paramedian	IVD level	IV	S1 (left and right)
HLS.062	L4-L5	Protrusion	Paramedian/Foraminal	IVD level	III	L4 (right)
	L5-S1	Protrusion	Paramedian	IVD level	III	S1 (left)
HLS.063	L3-L4	Protrusion	Foraminal	IVD level	IV	L3 (right)
HLS.064	L3-L4	Sequestration	Paramedian	Ascending	III	L3 (right)
HLS.067	L2-L3	Extrusion	Paramedian	Descending	IV	L3 (right)
HLS.070	L3-L4	Prolapse	Foraminal	IVD level	III	L3 (left)
	L4-L5	Extrusion	Paramedian	Descending	III	L4 and L5 (left)
	L5-S1	Prolapse	Paramedian/Foraminal	Descending	IV	L5 and S1 (right)
HLS.072	L5-S1	Protrusion	Median/Paramedian	IVD level	II	S1 (right)
HLS.075	L5-S1	Extrusion	Paramedian/Foraminal	IVD level	III	S1 (left)

In the set of 14 LDHs, there were 3 prolapsed LDHs, 6 protruded LDHs, 4 extruded LDHs and 1 sequestrated LDH. Regarding the LDH topography, there were 2 Median/Paramedian LDHs, 6 Paramedian LDHs, 4 Paramedian/Foraminal LDHs and 2 Foraminal LDHs. In terms of location, there were 5 descending LDHs, 8 LDHs at the level of the IVD and 1 ascending LDH. Concerning the Pfirrmann's Grade, there was 1 Grade II, 8 Grade III and 5 Grade IV IVD degeneration.

4.2 Relation between NPRS/ODI and age, sex, BMI and LDH area

4.2.1 NPRS

In order to analyse the NPRS in conjunction with some socio-demographic data, such as age, sex, BMI and LDH area, the data in Table 4.2 should be taken into account.

Table 4.2 – Socio-demographic data and LDH area per patient and per IVD.

HLS	IVD	Age (years)	Sex	BMI (kg/m^2)	BMI Classification	LDH area (mm^2)	NPRS Axial Basal	NPRS Axial Peak	NPRS Radicular Basal	NPRS Radicular Peak	ODI total
HLS.053	L4-L5	56	M	29.1	Overweight	76,83	0	0	4	8	78
HLS.055	L5-S1	49	F	25.9	Overweight	86,10	0	0	4	10	42
HLS.056	L4-L5	50	M	37.7	Obesity Grade II	83,53	0	0	4	9	38
	L5-S1					27,10					
HLS.062	L4-L5	67	F	30.5	Obesity Grade I	55,27	0	0	0	0	28
	L5-S1					24,80					
HLS.063	L3-L4	57	M	38.7	Obesity Grade II	37,37	0	0	6	8	52
HLS.064	L3-L4	54	M	28.7	Overweight	236,40	0	3	0	7	52
HLS.067	L2-L3	75	F	22.1	Normal Weight	90,97	4	8	4	9	50
HLS.070	L3-L4	59	F	39.8	Obesity Grade II	59,57	0	0	8	10	58
	L4-L5					122,57					
	L5-S1					51,30					
HLS.072	L5-S1	28	F	20.2	Normal Weight	48,83	0	0	8	10	48
HLS.075	L5-S1	43	F	27.3	Overweight	88,33	0	0	8	10	48

All individuals, except HLS.064 and HLS.067, rated axial pain as 0; this means that they do not had pain centred in or around the spine. On the other hand, patient HLS.064 rated basal pain as 0 and peak pain as 3, while patient HLS.067 rated basal pain as 4 and peak pain as 8. Relating axial pain to the LDH area, patient HLS.064 had the largest LDH and may therefore

experience mild to moderate back pain, whereas patient HLS.067 had the third largest LDH in the group and experienced pain from moderate (basal) to very strong (peak).

Moving on to radicular pain, all patients except HLS.062 reported some level of radiating pain. Patient HLS.062 does not reported radiating pain, despite having 2 LDHs, one of which is at L5-S1 (the smallest LDH in the study), which compresses the left nerve root, the same side where the patient's symptoms are located. Patient HLS.064, although having the largest LDH, reported a NPRS score of 0-7 (basal/peak), indicating strong to very strong pain at its peak, which demonstrates an apparent contradiction between the size of the LDH and the intensity of the pain. Patient HLS.063, with the third smallest LDH, rated the NPRS as 6-8, possibly influenced by his high BMI (Obesity Grade II). This may indicate that even with a small volume of LDH, weight may affect the pain the patient experiences. Finally, patients HLS.070, HLS.072 and HLS.075 reported the highest pain intensity, with NPRS of 8-10 (very strong to maximum pain). Among them, patients HLS.072 and HLS.075 are the youngest and are both female, suggesting a possible lower tolerance for pain. The youngest patient in the study (HLS.072) had the fourth smallest LDH, while the second youngest patient (HLS.075) had the fourth largest LDH in the study, suggesting a contradiction between age, LDH area and pain level. Patient HLS.070 experienced pain on the left side and had an L4-L5 LDH (left) which corresponds to the second largest LDH in the group, as well as an L3-L4 LDH (left) that had a larger area than the LDH on the right. Consequently, this patient experienced greater pain, as in addition to having Obesity Grade II, they had the highest number of LDHs and one of their LDHs had a large volume.

The outputs obtained from radicular pain seems to suggest a relation between age and the NPRS, since the youngest patients were the ones with the most pain. However, the oldest patient presented a radicular pain score of 4-9, while the second oldest patient (HLS.062) had no symptoms at all. Therefore, there is no sufficient evidence to establish any correlation between age and pain intensity. Regarding sex, women tend to report higher levels of pain on the NPRS scale compared to men, although this difference is not statistically significant for this number of cases. Regarding BMI, it does not seem to be related to the NPRS, as the patient with the highest BMI (HLS.070) reported a pain score of 8-10 and the patient with the fourth highest BMI (HLS.062) was asymptomatic. Furthermore, patient HLS.072 had a NPRS pain score of 8-10 and had a normal weight. Lastly, in terms of LDH area, the smallest LDH in the study corresponds to patient HLS.062, who had no symptoms on the NPRS scale for both axial and

peak pain, which seems to suggest that the smaller LDHs are associated with fewer symptoms. There are still contradictory outputs, as patient HLS.064 had the largest LDH and rated their pain as 0-7, and it would be expected that this patient would report a higher level of pain on the NPRS; patient HLS.070, who had the second largest LDH, had symptoms on the NPRS ranging from 8 to 10, which is more aligned with the overall behaviour observed in this sample.

4.2.2 ODI

The study sample consists of 10 patients, 2 of which had moderate disability and are still abled to performed most of their daily activities with few limitations caused by LBP; 7 patients had severe disability, which significantly impacts their daily activities and 1 patient had extreme back pain, meaning that the patient is severely incapacitaded and likely dependent on others for daily activities. Appendix 2 shows that the task considered least demanding for the patients was walking. The tasks considered to be most demanding, and such as were rated as significantly difficult, were pain intensity, weightlifting, social life and traveling. The remaining tasks (sitting, sex life, sleeping, personal care and standing, respectively) were rated as having moderate difficult.

The ODI score does not seem to be correlated with age, as the second oldest patient had the lowest disability, while the oldest patient had a score closest to the average score for the group (severe disability). Previous studies suggested that older patients tend to have a higher ODI scores, since with ageing there is a greater likehood of IVD degeneration and other associated conditions, resulting in increased disability [48].

The ODI score seems to be correlated with sex, as the first, third and fourth patients with the highest scores are male. There is one more male patient, but he had the second lowest ODI score, which may correspond to an outlier, the remaining patients are all female.

On the contrary, the ODI score doesn’t seem to be correlated with BMI, because although the 2 patients with the highest BMI were the second and third highest ODI scores, the third highest BMI patient had the second lowest ODI score.

The ODI score also seems to be correlated with the area of the LDH, as the 2 patients with the smallest LDHs were in the moderate disability group, while the patients with the largest LDHs correspond to the second and third patients with the highest ODI scores and were

therefore part of the severe disability group. This can be explained by the fact that larger LDHs or those that significantly compress nerve roots are associated with higher levels of pain and consequently, greater disability.

4.3 IVD height comparison: Healthy vs LDH patients

In this subchapter, the average anterior and posterior heights of each lumbar IVD measured by MRI in patients HLS.053, HLS.055, HLS.062, HLS.067 and HLS.070 (Appendix 7), will be compared with the average anterior and posterior heights of each lumbar IVD by MRI in a study of 171 patients [45]. The patients in this study were chosen because they had different analyses and correlations from the others. In detail, this study analysed the average anterior and posterior heights, organised by sex and age group, as shown in Appendix 8. Analysis of this data revealed that IVD height increases as one moves down the spine, as the lower IVDs tend to be thicker to support greater load and pressure. However, from L4-L5 to L5-S1, there is typically a decrease in height, which can be explained by the transition from the lumbar spine to the sacrum. Additionally, it is observed that the anterior height is always greater than the posterior height, as a result of lumbar lordosis. Loss of stature occurs with increasing age, and as a result, there tends to be a decrease in IVD height due to dehydration, loss of elasticity and reduced shock absorption capacity.

Comparing the IVD heights of patient HLS.053 with the IVD heights of healthy 56 year old male patients, it was observed a decreased by approximately 1 mm in the anterior height of the IVDs from L1-L2 to L4-L5 and a decreased about 3 mm at L5-S1 in the patient. The posterior heights of the IVDs were quite similar to those of healthy patients. The herniated L4-L5 showed no significant changes in IVD height compared to healthy patients. The patient reported moderate to very severe radicular pain (radicular NPRS 4-8) and had an ODI score of 78, indicating disabling back pain and significant difficulty in daily activities. Although the minimal reduction in IVD height, the extruded LDH may be significantly compressing the nerve roots in this region, which explains the intensity of the pain and the high degree of disability experienced by the patient.

Patient HLS.055 (female, 49 years old) showed a decreased of approximately 2 to 3 mm in the anterior height of the IVDs from L1-L2 to L3-L4 and a more pronounced reduction of 6

mm at the L5-S1. The posterior heights of the IVDs were similar to those of healthy patients. The significant decreased in the height of the L5-S1 may be attributed to loss of water content, which can cause instability and increased pressure on the IVD and joint structures. Even with a preserverd posterior height, the presence of a posterior herniation can directly compress the nerve roots in the L5-S1 region, potentially causing sciatica. The patient reported radicular pain ranging from moderate to extremely intense (radicular NPRS 4-10), possibly related to the decreased in anterior IVD height. The ODI score of 42 indicates severe disability, suggesting a significant impact on the patient's daily activities and quality of life, even though the pain measured by NPRS is not consistently extreme.

Patient HLS.062 showed a decreased of approximately 1 mm in the anterior height of the L4-L5 and L5-S1 compared to healthy 67 year old females, while the other IVDs maintained similar heights. On the posterior side, the heights were similar to those of healthy patients, except for the L4-L5, which shows a reduction of around 5 mm. Despite the changes in the anterior height of herniated IVDs (L4-L5 and L5-S1), the patient reported no pain on the radicular NPRS, suggesting that there was no significant nerve root compression, possibly due to the small size of the L5-S1 LDH. The 5 mm difference in posterior height of the L4-L5 compared to healthy patients may contributed to overload in the joints and muscles of the spine, causing discomfort when performing physical activities. In terms of the ODI, the patient had a total score of 28, indicating low moderate disability, reflecting some limitations in daily activities while still maintaining a reasonable level of functionality.

In patient HLS.067, there was an increased by approximately 2 mm in the anterior height of the L1-L2 and L2-L3, while the L3-L4 showed a decreased by 3 mm. On the posterior side, the L1-L2, L3-L4 and L5-S1 increased by around 2 mm, 2 mm and 1 mm, respectively. Regardind the herniated IVD, the anterior height increased by approximately 2 mm, but the posterior height remained pratically the same as in healthy individuals. On the radicular NPRS, the patient rated the pain between 4 and 9, indicating that the LDH may be compressing the nerve roots, causing significant radicular pain. The unchanged posterior height in LDH (L2-L3) suggests that the nerve compression is not caused by the IVD height, but rather by the presence of an extruded LDH, which displaces the IVD material. The increased in anterior height indicates that the IVD may be under greater pressure, generating biomechanical imbalances. At ODI level, the patient had a total score of 50, reflecting severe disability, impacting their ability to move, sit or preform daily tasks.

Finally, in patient HLS.070, there was a decreased of approximately 4 mm in the anterior height of the L2-L3 IVD and a descreased of 5 mm in the L4-L5 and L5-S1. On the posterior side, there was a reduction of around 3 mm in L2-L3 and 2 mm in L5-S1, while the L3-L4 showed an increased of approximately 1 mm compared to healthy patients. The decreased in anterior height in the L4-L5 and L5-S1 indicates significant IVD degeneration, which can cause a significant biomechanical imbalance and overload adjacent structures, increasing spinal instability. On the radicular NPRS scale, the patient rated the pain between 8 and 10, which can be explained by the presence of 3 LDHs and nerve compressions at different levels. The combination of mechanical compression, inflammation and severe IVD degeneration outputs in persistent and severe pain, especially at the lower levels, which are particularly vulnerable to nerve compression. At ODI level, the patient obtained a total score of 58, reflecting a severe disability that significantly limits the performance of daily activities such as walking, standing, sitting, among others.

4.4 Analysis by imaging modality

4.4.1 MRI

Table 4.3 shows the average anterior, central and posterior heights of each IVD in the sagittal plane and the average left, central and right heights of each IVD in the coronal plane, for all 10 patients with MRI scans.

Table 4.3 – Average IVD heights in MRI.

MRI IVD height (mm)						
IVD	**Sagittal Plane**			**Coronal Plane**		
	Anterior	**Central**	**Posterior**	**Left**	**Central**	**Right**
L1-L2	9.21 ± 1.64	10.70 ± 1.56	7.25 ± 1.25	11.24 ± 0.99	10.65 ± 0.61	10.86 ± 1.46
L2-L3	10.13 ± 1.61	10.98 ± 1.47	7.49 ± 1.19	11.25 ± 1.52	11.92 ± 0.95	11.19 ± 0.75
L3-L4	11.73 ± 1.39	12.36 ± 1.48	8.15 ± 0.90	11.53 ± 1.40	12.22 ± 1.08	11.01 ± 0.84
L4-L5	12.87 ± 2.49	11.56 ± 2.44	7.49 ± 1.60	10.84 ± 0.67	12.93 ± 0.99	10.01 ± 1.23
L5-S1	12.35 ± 2.48	10.21 ± 2.33	6.90 ± 0.93	-	-	-

In the sagittal plane, it can be observed that the height of the IVDs varied according to their position (anterior, central and posterior) at each level, with greater IVD height on the central (L1-L2 to L3-L4) or anterior (L4-L5 and L5-S1) side and less on the posterior side. Across the various levels, the average IVD height in the anterior and central positions ranged from 9 to 12

mm, while in the posterior side it was approximately 7 mm, which can be explained by lumbar lordosis. In addition, it was noted that from L1-L2 to L4-L5, the heights tend to increased, whereas from L4-L5 to L5-S1, the heights tend to decreased slightly. It is also evident that the L5-S1 had the lowest central and posterior height, indicating that the IVD was thinner in that region. In the coronal plane, there was a notable absence of values for the L5-S1, as it is not visible in this plane due to the transition from the lumbar spine to the sacrum. Thus, analysing the L1-L2 to L4-L5 levels, the average IVD heights varied from 10 to 12 mm, with small variations between the left, central and right positions, with the central positions generally being slightly higher.

Table 4.4 contains the average anterior, central and posterior heights of the vertebrae in the sagittal plane, as well as the average left, central and right heights of vertebrae in the coronal plane.

Table 4.4 – Average vertebral heights on MRI.

MRI vertebral height (mm)						
Vertebra	**Sagittal Plane**			**Coronal Plane**		
	Anterior	**Central**	**Posterior**	**Left**	**Central**	**Right**
L1	25.30 ± 2.13	24.18 ± 2.27	26.31 ± 2.37	24.63 ± 1.14	24.07 ± 1.68	24.66 ± 1.45
L2	26.98 ± 2.10	24.54 ± 1.75	27.63 ± 2.44	25.13 ± 1.24	24.47 ± 2.87	24.80 ± 1.45
L3	28.08 ± 1.90	23.92 ± 0.98	26.64 ± 2.24	24.70 ± 1.66	24.19 ± 1.53	25.19 ± 1.77
L4	27.43 ± 2.00	23.93 ± 1.65	26.63 ± 2.18	26.22 ± 1.85	24.03 ± 1.20	25.63 ± 2.95
L5	28.55 ± 2.11	23.63 ± 2.30	24.24 ± 1.15	27.70 ± 1.95	27.40 ± 1.80	27.28 ± 1.62
S1	31.88 ± 2.42	26.18 ± 3.17	25.25 ± 2.94	-	-	-

Analysing the table, it is observed that the average height of the L1 to L5 vertebrae on the anterior side was approximately 27 mm, in the central position it was approximately 24 mm and in the posterior side it was approximately 26 mm. Furthermore, the anterior and posterior heights of the vertebrae from L1 to L5 do not varied much within the same level and were consistently greater than the central heights. Moving to the S1 vertebra, the anterior height was significantly greater than in the lumbar vertebrae, reflecting the different function and greater load supported by the sacral region; the central height was greater compared to the lumbar vertebrae, but less than the anterior height, while the posterior height was the smallest of the 3 measurements for S1. In the coronal plane, the heights of the vertebrae from L1 to L4 were similar, with the average left and right heights being approximately 25 mm and the average central height about 24 mm. In addition, it was noted that the heights tend to increased

progressively from L1 to L4. The L5 vertebra stands out from the others, as it had height of approximately 27 mm.

In terms of the intervertebral angles, in 2D, the average outputs for each IVD are shown in Table 4.5. Analysis of the outputs showed that the intervertebral angles in the sagittal plane progressively increased from L1-L2 to L5-S1 (Figure 4.1), indicating a greater inclination in this plane as one moves down the lumbar spine. This result was consistent with the function of load absorption and movement of the lumbar spine. The intervertebral angles in the coronal plane reflected the inclination or rotation of the spine in that plane, usually described as scoliosis, and as such, are quite different and lower than the angles in the sagittal plane.

Table 4.5 – Mean intervertebral angles in MRI.

MRI Intervertebral Angle (°)		
IVD	**Sagittal Plane**	**Coronal Plane**
L1-L2	3.34 ± 2.06	1.07 ± 0.86
L2-L3	4.65 ± 2.98	2.46 ± 1.75
L3-L4	6.65 ± 2.17	2.23 ± 1.19
L4-L5	10.25 ± 3.29	1.93 ± 1.37
L5-S1	11.73 ± 5.81	-

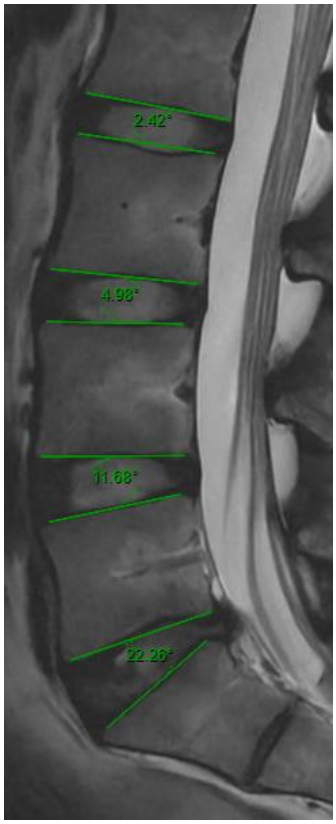

Figure 4.1 – Intervertebral angles measured in L2-L3, L3-L4, L4-L5 and L5-S1 levels in sagittal plane of patient HLS.072.

Regarding the length of the herniated IVD, the average value was 45.48 ± 4.90 mm; the average value of the lumbar lordosis angle was 48.21 ± 8.57°; the average area of the IVD without the LDH was 365.24 ± 68.57 mm^2 and the average area of the LDH was 77.78 ± 51.37 mm^2.

4.4.2 CT

Appendix 3 contains the tables with the average values of each parameter measured on the CT scans (2D), specifically the table of average IVD and vertebral heights, as well as the table of average intervertebral angles, for the 4 patients who underwent this examination.

The analysis of the average IVD heights in the sagittal plane reveals that the L1-L2 and L2-L3 had the highest central height, while the posterior height was the lowest. At the L3-L4, L4-L5 and L5-S1 levels, the anterior height was greatest, followed by the central height and finally the posterior height (Figure 4.2). On average, the anterior and central heights of the IVDs were approximately 9 mm, while the posterior height was around 4 mm. There was also a tendency of increasing anterior and posterior IVD heights from the L1-L2 level to L4-L5. The L5-S1 had the lowest central height, but still had a relatively high anterior height, as its morphology is different from the other IVDs. In the coronal plane, the average heights of the IVDs on the left and right sides were about 7 mm, with the central height approximately 9 mm, indicating a greater concentration of load on the sides of the IVDs. At the L1-L2 and L2-L3 levels, the heights were similar to each other on the various sides, but at the L4-L5 level, there was a significant discrepancy between the central and lateral heights, suggesting IVD asymetry.

Figure 4.2 – IVDs heights measured in L3-L4, L4-L5 and L5-S1 levels in sagittal plane of patient HLS.053.

The average height of the vertebrae was approximately 30 mm at the anterior part, 26 mm in the central part and 29 mm in the posterior part. In the L1 and L2 vertebrae, the posterior heights were greater than the anterior and central heights, which is common at the beginning of the lordotic curve, while in the L3 to S1 vertebrae, the anterior height was greater than the posterior height. The L5 and S1 vertebrae exhibited lower posterior heights compared to other levels, due to pronounced lumbar lordosis or degenerative processes. Additionally, the L5 vertebra had a reduced central and posterior heights, suggesting a marked anterior curvature. On the other hand, the S1 vertebra had the highest anterior height, which was consistent with its load-bearing function. In the coronal plane, the average heights on the left and right sides were about 29 mm, with the average central height at 26 mm, demonstrating symmetry in vertebral shape. It is also noted that the central height in all vertebrae, was always lower than the lateral heights, as the lateral heights are higher to support the vertebral arch. Vertebral height increased progressively from L1 to L4, but in the L5 vertebra there was a reduction in height on all sides, which may be related to the transition from the lumbar spine to the sacrum and to the compressive forces in that region.

The average intervertebral angle in the sagittal plane was approximately 9º, while in the coronal plane it was around 1º. In sagittal plane, the intervertebral angles increased from L1-L2 to L4-L5, reflecting the typical lordotic curve of the lumbar spine. At the L5-S1 level, the intervertebral angle decreased slightly but remains high, characteristic of the transition to the sacral region, where the spines begin to curve again. The intervertebral angles in the coronal plane are significantly smaller, indicating a slight lateral inclination of the vertebrae, which should be minimal since the spine is more vertically aligned in this plane.

Finnaly, in terms of the length of the herniated IVD, the mean value obtained was 47.65 ± 4.66 mm and the mean value of the angle of lumbar lordosis was 52.16 ± 8.42°.

4.4.3 Standing X-ray

Appendix 4 contains the tables with the mean values of each parameter measured on the Standing X-ray of the 9 patients who underwent this examination.

Analysis of the average values of IVD height shows that the average anterior height was approximately 15 mm, while the average posterior height was around 9 mm, with the anterior

height consistently greater at all levels. Anterior height increases from L1-L2 to L3-L4, reflecting the need for greater support and mobility in the lower part of the lumbar spine, which bears more load. After L3-L4, the anterior height decreased slightly, but was still significant for supporting weight and allowing flexibility in the transition to the sacrum. The posterior height of the IVDs varied less, as the lumbar curvature is accentuated in the anterior portion, keeping the posterior part relatively aligned. The left and right IVDs heights were approximately 8 mm, suggesting symmetry at most levels, with small differences that may be physiological or result from postural variations. At the L2-L3 and L4-L5 levels, the left height was greater than the right, while the opposite was true for the other IVDs and these variations can be attributed to slight postural misalignment or asymmetric IVD compression.

The average anterior height of the vertebrae L1 to L5 was approximately 37 mm and the average posterior height was around 34 mm. At L1 and L2, the posterior height was greater than the anterior height due to a slight posterior concavity, which is common at the beginning of the lordotic curve. In L3, the difference between anterior and posterior heights was minimal, refleting the transition between the upper and lower parts of the lumbar spine. From L5 to S1, the height difference increased, characterising the greater inclination and curvature of lower lumbar region. The S1 vertebra had the highest anterior height, related to its role in supporting body weight and the transition between the spine and pelvis. The discrepancy of around 7 mm between the anterior and posterior heights of L5 may indicate hyperlordosis. In the coronal plane, the average left and right heights of the vertebrae were approximately 31 mm, with very similar heights on both sides, indicating significant symmetry and good alignment along the lumbar spine, with no obvious signs of scoliosis.

The intervertebral angle on the Standing X-ray was only measured in the sagittal plane, as mentioned in the Methodology. The average intervertebral angle was approximately 9º and progressively increased as one descends the lumbar spine, reflecting a healthy lumbar lordosis. Consequently, the L1-L2 and L2-L3 levels had the smallest angles, indicating a less pronounced curvature at these higher levels. From L3-L4, there was a considerable increase in the angle, which reflects the beginning of the most curved part of the lumbar lordosis. The L4-L5 and L5-S1 levels had the largest angles.

Finally, the average lumbar lordosis angle was 56.17 ± 12.99°, the average area of the foramen containing the LDH was 138.08 ± 43.06 mm^2 and the largest diameter of the foramen was 20.30 ± 2.54 mm.

4.4.4 Functional X-ray

Appendix 5 shows the tables with the average values of each parameter measured in the Functional X-ray of the 8 patients who underwent this exam.

In extension, the average anterior height was approximately 15 mm and the average posterior height was about 8 mm, showing a significant difference, especially at the lower levels of the spine. This occurs because in extension, most of the load is transferred to the posterior part of the spine, causing increased stress on the facet joints and ligaments. The anterior height was consistently greater than the posterior height, because in a position of spinal extension, the posterior part of the IVD is compressed and the anterior part is extended. The increased in anterior IVD height and posterior compression at L5-S1 indicate that this region bears most of the mechanical stress during extension, which may predispose this area to IVD degeneration and, consequently, the development of IVD herniations and root compressions. In flexion, the average anterior height of the IVD was approximately 13 mm, while the posterior height was around 9 mm. During flexion, IVDs tend to decrease their anterior height and increase their posterior height, compared to extension. The posterior height of the IVDs between L1-L2 and L4-L5 remained stable, indicating less flexion at these levels, which is in line with anatomy, as the upper IVDs have less mobility in flexion compared to the lower levels. In contrast, the posterior height of the L5-S1 was the lowest compared to the other levels, reflecting greater compression, as it supports a large part of the trunk's weight and is more susceptible to compression due to the curvature of lumbar lordosis and the biomechanics of flexion.

In both extension and flexion, the average anterior height of the vertebra was approximately 37 mm, while the average posterior height was around 35 mm. In extension, the vertebral heights showed a pattern of gradual increase from L1 to L5 on the anterior side. In the upper vertebrae, L1 and L2, the posterior height was greater than the anterior height, on the other hand, in the L3 to S1 vertebrae, the anterior height was greater than the posterior height. In flexion, in the L1 to L3, the posterior height was slightly higher than the anterior height, while

in the L4 to S1 vertebrae, the anterior height was significantly higher than the posterior height. At levels L1 to L4, the anterior and posterior heights were quite similar, however, at L5 and S1, there was a notable difference between the anterior and posterior heights, which may be normal depending on the flexibility of the spine.

The average intervertebral angle was approximately 11º in extension and about 6º in flexion. In both movements, there was a progressive increase in these angles as one moves down the lumbar spine, a characteristic pattern of a lordotic curve. The L4-L5 and L5-S1 levels had the largest angles, reflecting greater mobility and flexibility, but also greater susceptibility to problems such as instability and IVD degeneration. In contrast, the upper levels, L1-L2 and L2-L3, had smaller angles, conferring greater stability and less likelihood of injury. This gradual increase in angles suggests a balanced distribution of curvature along the lumbar spine, preventing excessive force concentration at any single level and protecting the spine from injuries, while at the same time allowing for mobility distribuction between several levels.

Finally, the average lumbar lordosis angle in extension was 65.24 ± 9.87º and in flexion was 38.63 ± 18.14º. This reduction in the angle was consistent with the expected during the flexion movement, where the lordotic curvature is attenuated. In terms of the area of the foramen containing the LDH, in extension it had a mean value of 155.56 ± 44.78 mm^2 and in flexion 194.78 ± 69.04 mm^2, while the largest diameter of the foramen was 22.74 ± 5.50 mm in extension and 24.28 ± 6.50 mm in flexion. During flexion, the expanded foramen space can alleviate nerve root compression, often providing symptom relief. Conversely, extension narrows the foramen, potentially exacerbating pain. This biomechanical relationship explains why sciatica patients might adopt a forward-bending posture to reduce discomfort and why tests like the Straight Leg Raise Test reproduce symptoms by stretching the nerve. Such dynamics highlight the correlation between nerve impingement and adaptative gait patterns to minimize pain.

4.4.5 3D models

In terms of 3D models, Appendix 6 contains the tables with the average values of each parameter measured in the 3D models for the 4 patients with CT scans.

Considering the sagittal plane and all levels, the average anterior height of the IVD was approximately 9 mm, central height was 8 mm and posterior height was 4 mm. Additionally,

there was a noticeable transition in the distribution of IVD heights, i.e. at the L1-L2 and L2-L3 levels, the central height was the greatest, followed by the anterior and posterior heights. On the other hand, at the L3-L4 to L5-S1 levels, the order reverses, with the anterior IVD height becoming the largest, followed by central and posterior. There was also a trend of increasing anterior and posterior heights from L1-L2 to L4-L5. The L5-S1 had the lowest central height, but maintains a significant anterior height, suggesting possible central compression or wear due to increased load at this level. In the coronal plane, the average heights were approximately 6 mm (left), 8 mm (central) and 7 mm (right). The L1-L2 and L2-L3 levels showed similar heights on all sides, while L3-L4 and L4-L5 levels exhibited significant discrepancies between central and lateral heights, possibly indicating IVD lateral inclinations or rotation.

In terms of vertebral height, in the sagittal plane, the approximate average heights were: anterior 31 mm, central 27 mm and posterior 29 mm. Analysis of the outputs showed that the L1 and L2 vertebrae had the greatest posterior height, while L3 and S1 had the greatest anterior height. The L5 and S1 vertebrae had the lowest posterior heights. Additionally, L5 had reduced central and posterior heights, indicating a significant anterior curvature, while S1 had the highest anterior height, consistent with its supportive function. In the coronal plane, the average lateral heights were approximately 29 mm, with a central height of about 26 mm. In this plane, there was symmetry between the left and right sides, with the central height always being lower. A progressive increased in height from L1 to L4 was also observed, followed by a reduction at L5, possibly related to the lumbosacral transition.

The average intervertebral angles in the sagittal plane were approximately 9º, while in the coronal plane, they were around 2º. In the sagittal plane, the angles progressively increased from L1-L2 to L4-L5, reflecting the typical lordosis of the lumbar spine, with a slight decreased at L5-S1, which marks the transition to the sacral region. In the coronal plane, the angles were significantly lower than those in the sagittal plane, indicating a slight lateral inclination of the vertebrae. Lastly, the average of lumbar lordosis angle was 54.03 ± 7.46°.

4.5 Differences between imaging modalities

In this subchapter, the sample was divided into two groups: Group 1 – 8 patients with Functional X-ray as well as MRI and Standing X-ray, and Group 2 – 4 patients with the 4 exam

modalities. The parameters analysed were IVD height, vertebral height, intervertebral angle and lumbar lordosis angle, measured in the sagittal plane, as these are the common parameters obtained from all imaging techniques and 3D models.

4.5.1 Comparison with MRI

First, it was necessary to calculate the percentage deviation between MRI and another imaging modality for a paramenter for each IVD/vertebra in each patient. Then, for each parameter, the number of percentage deviations for each combination of exams was counted, totalling the patients in each group, along with the number of positive/negative deviations, which were then converted into a percentage. In this way, if a percentage deviation was negative, it means that the parameter analysed in MRI is lower than the same parameter in other imaging modality.

At the vertebral height level, it was found that Group 1 showed 100% of the values in Standing and Functional X-ray higher than in MRI. On the other hand, in Group 2, it was concluded that approximately 97% of the values in CT were higher than in MRI, 100% of the values in Standing and Functional X-ray were higher than in MRI and about 99% of the values in 3D models were higher than in MRI. In CT and both X-rays, the bone structures are more visible, so a possible explanation for this outcome may be related to a slight increase in height of the vertebra in these scans when compared to MRI. The same is true for 3D models, which are based in CT scans. However, the vertebral height should be similar in all imaging techniques, regardless of the position or movement performed.

Moving on to IVD height, in Group 1, it was observed that in Standing and Functional X-ray exams, this height was approximately 87% and 81%, respectively, higher when compared to MRI. This suggestion seems inconsistent with the literature, as the transition from a supine to standing position should lead to compression of the IVDs and, consequently, a decrease in IVD height [49]. In Group 2, approximately 93% of the values in CT were lower than the MRI values and 100% of the values in 3D models were lower than in MRI, which proves what is described in the literature, since the IVDs are more visible in the MRI, so the IVD height in the MRI tends to be higher [50]. However, in Standing and Functional X-ray, the IVD height was approximately 95% and 88% (extension) and 85% (flexion) of the time, respectively, higher when compared to MRI, which once again seems inconsistent with the literature [49]. This

contradiction may be due to the state of IVDs hydratation, because if the MRI scan was carried out after a period of weight-bearing, the IVDs will show less height when compared to a X-ray scan. In addition, the patient's position can influence the height of the IVD, because if the patient is in a position that favours the opening of the intervertebral joints (such as flexion or extension), the height of the IVD may appear higher on the MRI. In X-ray techniques there is an overlapping of layers, which can result in an altered representation of the IVD height, reflecting an incorrect IVD height. The image quality of X-ray techniques is much lower than that of MRI for analyzing the IVD. X-ray IVD height is determined by the distance between two vertebrae, which can obscure details about the IVD structure and lead to incorrect IVD height measurements. In addition, depending on the angle and technique used in the X-ray, the height of the IVD can be exaggerated, for example, if a projection is not aligned correctly, it can give the impression of greater height due to the perspective.

In terms of intervertebral angle, in Group 1, in Standing and Functional X-ray exams, this angle was approximately 65% (in standing), 78% (extension) and 50% (flexion), respectively, higher when compared to MRI. In Group 2, it was concluded that in CT scans and 3D models, the intervertebral angles were 85% and 80% higher, respectively, when compared to MRI. On the other hand, in the Standing and Functional X-ray (only at the flexion level), these angles were 55% higher and lower, respectively. Finally, in Functional X-ray (at extension level), 70% of the intervertebral angles were higher than in MRI. Similar outputs to MRI should be observed in both CT and 3D models, however, in Standing and Functional X-ray (extension), the angles should be higher, while in flexion, the angles should be lower [51].

Finally, the lumbar lordosis angle in Group 1 showed the following outputs: approximately 88% of the values in Standing X-ray were higher than in MRI; 100% of the values in Functional X-ray (extension) were higher than in MRI and 75% of the values in flexion were lower than in MRI. These outputs are aligned with the literature, as the lumbar lordosis angle tends to increase in extension and decrease in flexion when compared to MRI [51]. In Group 2, it was concluded that in both CT and Standing X-ray exams, as well as in 3D models, 75% of the lumbar lordosis angles were higher compared to MRI. In the Functional X-ray exam at the extension level, all the lumbar lordosis angles were higher than those in MRI, while in flexion, 75% of the lumbar lordosis angles were lower than those obtained in MRI.

4.5.2 Analysis of the average deviations in each IVD/vertebra

After calculating the percentage deviation between MRI and another imaging modality for each IVD/vertebra, in each patient, the average percentage deviation for each IVD/vertebra per parameter was calculated for the total number of patients in each group.

4.5.2.1 Vertebral height

From the analysis of Appendix 9, referring to Group 1, in Standing and Functional X-ray (extension), it was noted that the greatest percentage deviation occured in the posterior part of the vertebra in the L1, L2, L3 and S1 vertebrae, while in the L4 and L5 it occured in the anterior part. In the flexion movement, in all vertebrae except L5, the greatest percentage deviation occured at the posterior part of the vertebra, while in the L5 vertebra, the greatest percentage deviation occured in the anterior part.

In Group 2, based on Appendix 10, in CT and 3D models, it can be seen that in the vertebrae L1, L2 and L3, the greatest percentage deviation occured in the posterior part, unlike the other vertebrae, where it occured in the central part. In Standing and Functional X-ray (extension), the greatest percentage deviation occured at the posterior part of the L1, L2, L3 and S1, while in the L4 and L5 vertebrae, it occured in the anterior part. In flexion, the vertebrae L1, L3, L4 and S1 showed the greatest percentage deviation on the posterior side, while the other vertebrae showed the greatest deviation on the anterior side.

Thus, it can be seen that, for vertebral height, the posterior side had the greatest percentage deviations. In addition, the percentage deviations between MRI and CT and 3D models tended to be lower compared to the other combinations of exams, indicating that both modalities provide relatively similar outputs in the assessment of vertebral height.

4.5.2.2 IVD height

In Appendix 9 (Group 1), both the Standing and Functional X-ray (extension) showed that the greatest percentage deviation, when compared to MRI, occured at the posterior part of the L4-L5, unlike the other IVDs, where the percentage deviation occured at the anterior part.

Regarding Functional X-ray (flexion), it was concluded that in all IVDs except L3-L4, the greatest percentage deviation occured in the posterior part of the IVD.

Analysing the outputs of Group 2, both in CT and 3D models, it was concluded that the greatest percentage deviation occured at the posterior part of all IVDs. In Standing X-ray, the greatest percentage deviation occured in the anterior part of the L1-L2 to L3-L4, while in the L4-L5 and L5-S1, it occured at the posterior part. In Functional X-ray (extension), the greatest percentage deviation occured in the posterior part of the L4-L5, unlike the other IVDs, which showed the greatest percentage deviation in the anterior part. On the other hand, in flexion, it was observed that the greatest percentage deviation occured in the posterior part of the L1-L2, L2-L3 and L4-L5, while the opposite was true for the other IVDs.

In extension, the anterior height of the IVDs tends to increase and the posterior height tends to decrease, when compared to the IVD height in MRI. In flexion, the anterior height of the IVD tends to decrease, while the posterior height tends to increase. Given this, the outputs obtained seem to be in line with the anatomy of the lumbar spine, as in the extension the greatest percentage deviation predominantly occured on the anterior side, while in flexion it occured on the posterior side. On the other hand, the Standing X-ray outputs did not seem to be in agreement with the literature [49], as transitioning from the supine to standing position should result in a decrease in IVD height and, consequently, positive percentage deviations. Additionally, it can also be seen that the percentage deviations in CT and 3D models were positive, while in Standing and Functional X-ray they were negative.

4.5.2.3 Intervertebral angle

From Appendix 9, related to Group 1, it was observed that in Standing and Functional X-ray (extension), the greatest percentage deviations were seen in the L1-L2 to L3-L4, all showed values below -100%. Conversely, in flexion, the greatest percentage deviations (< -100%) occured in the L1-L2 and L2-L3. Thus, it was verified that in Standing and Functional X-ray, the uppermost IVDs of the spine exhibited the greatest deviations. Additionally, the intervertebral angles in extension showed greater deviations than in flexion.

In Group 2 (Appendix 10), in CT and Standing X-ray, it was confirmed that the greatest percentage deviation occured in the L1-L2 and L3-L4, both of which were below -100%. In 3D

models, the only IVD with a percentage deviation of less than -100% was L3-L4. Regarding Functional X-ray (extension), the greatest percentage deviation occured in the L3-L4, which was the only deviation below -100%. In terms of flexion, the greatest percentage deviation occured in the L2-L3 and L4-L5, with both being close to 30%.

Additionally, it can be seen that for Group 1, the greatest percentage deviations occured in the L1-L2 and L2-L3 in terms of the intervertebral angle, while in Group 2 they mostly occured in the L1-L2 and L3-L4. Furthermore, in both Groups, it was noted that in most combinations, the L4-L5 exhibited the lowest percentage deviation. Additionally, it was evident that in Group 2, during flexion, the majority of the percentage deviations were positive.

4.5.2.4 Lumbar lordosis angle

Analysing Appendix 9, related to Group 1, it was observed that the percentage deviation between MRI and Functional X-ray (flexion) was the only positive deviation. Furthermore, comparing extension with flexion, it was concluded that the outputs obtained are aligned with the literature [51], as the lumbar lordosis angle tends to increase in extension (resulting in a negative percentage deviation) and decrease in flexion (resulting in a positive percentage deviation).

Regarding Group 2 and according to Appendix 10, it was concluded that the lowest percentage deviation occured between MRI and CT, while the largest deviation occured between MRI and Functional X-ray (extension). It can also be seen that the percentage deviation between CT and 3D model was similar. Just like in Group 1, Group 2 also showed that the percentage deviation in extension and flexion was as expected according to the literature [51].

4.5.3 Analysis of the number of IVDs/vertebrae/patients

Based on the percentage deviation between 2 imaging techniques, for each parameter, the number of IVDs (IVD height and intervertebral angles), vertebrae (vertebral height) and patients (lumbar lordosis angle) was evaluated within each percentage deviation, in the total number of patients per group. The percentage deviation intervals vary in increments of 20%, from $\Delta < -100\%$ to $\Delta > 100\%$.

Given that, each patient has a total of 6 vertebrae and 5 IVDs in the lumbar spine, Group 1 (8 patients) has 48 vertebrae and 40 IVDs and Group 2 (4 patients) has 24 vertebrae and 20 IVDs.

4.5.3.1 Group 1

Figure 4.3 shows the number of IVDs, at IVD height level, for each percentage deviation interval, according to the diferrent combinations of imaging techniques.

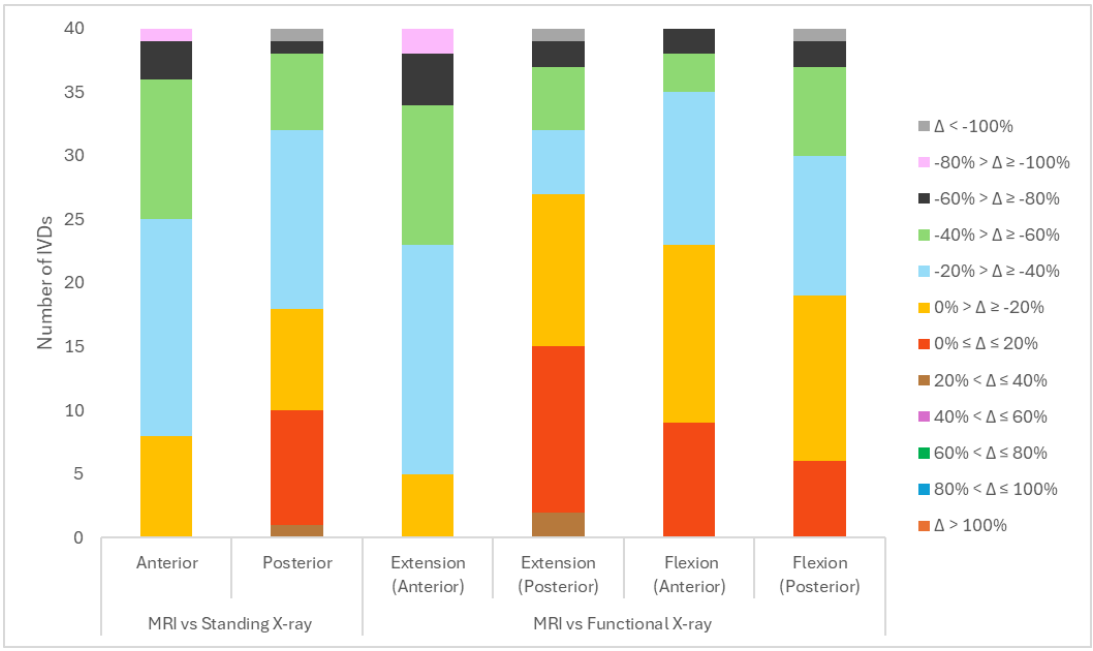

Figure 4.3 – Number of IVDs, for each percentage deviation interval, according to different combinations of imaging techniques, at IVD height level (Group 1).

From the analysis of Figure 4.3, it was observed that the IVDs exhibited a percentage deviation range from < -100% to 40% between the various combinations of exams, with the percentage deviation group with the highest number of IVDs being -20% > Δ ≥ -40%. Comparing MRI with Standing X-ray, it can be concluded that most of the differences were concentrated in negative values, suggesting that in general, MRI tends to have lower IVD heights than Standing X-ray. This result seems to be inconsistent with the literature [49], as seen before, as the transition from the supine to standing position should lead to compression of the IVDs and, consequently, a decrease in IVD height. Comparing Functional X-ray with

MRI, it was concluded that Functional X-ray was closer to MRI, as it exhibited fewer extreme deviations and showed a greater proportion of IVDs with small percentage difference.

Figure 4.4 illustrates the number of vertebrae at vertebral height level, according to the percentage deviation intervals and the combination of imaging modalities.

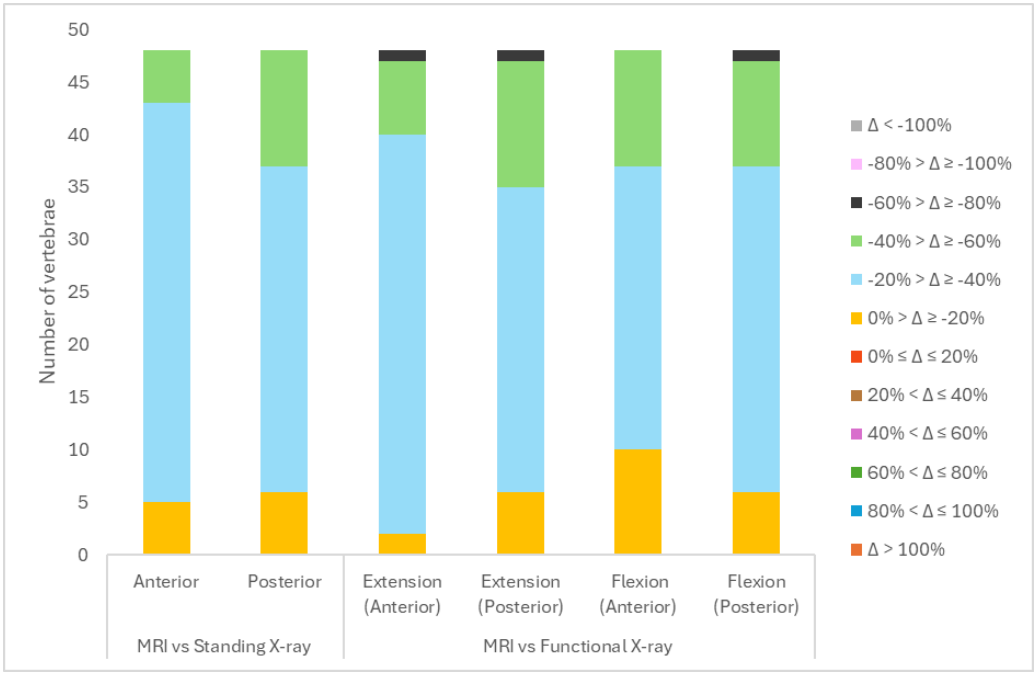

Figure 4.4 – Number of vertebrae, for each percentage deviation interval, according to different combinations of imaging techniques, at vertebral height level (Group 1).

At the vertebral height level, it was concluded that the variation in the percentage deviation was more moderate compared to the height of the IVD. Most of the vertebrae exhibited deviations in the -20% > Δ ≥ -40% interval, indicating a noticeable but not extreme difference. However, in Functional X-ray, there were a small number of vertebrae with larger deviations (-60% > Δ ≥ -80%), although this result is not significant. Thus, for vertebral height, MRI showed a relatively close correspondence with both Standing and Functional X-ray, with Standing X-ray having greater agreement with MRI.

Through the analysis of Figure 4.5, referring to the number of IVDs at intervertebral angle level, it was confirmed that there were a significant number of IVDs with very high deviations (Δ < -100%), suggesting that MRI tends to show considerably lower values when compared to Standing and Functional X-ray. Furthermore, the Δ > 100% interval was the only one that did

not include any IVDs. Thus, it was verified that the intervertebral angle was the parameter with the most discrepant values when compared to MRI values. This significant discrepancy may be due to the difference in patient posture, differences in imaging techniques, overlapping anatomical structures, different patient positions and movements, the quality of the images in each technique, among other aspects.

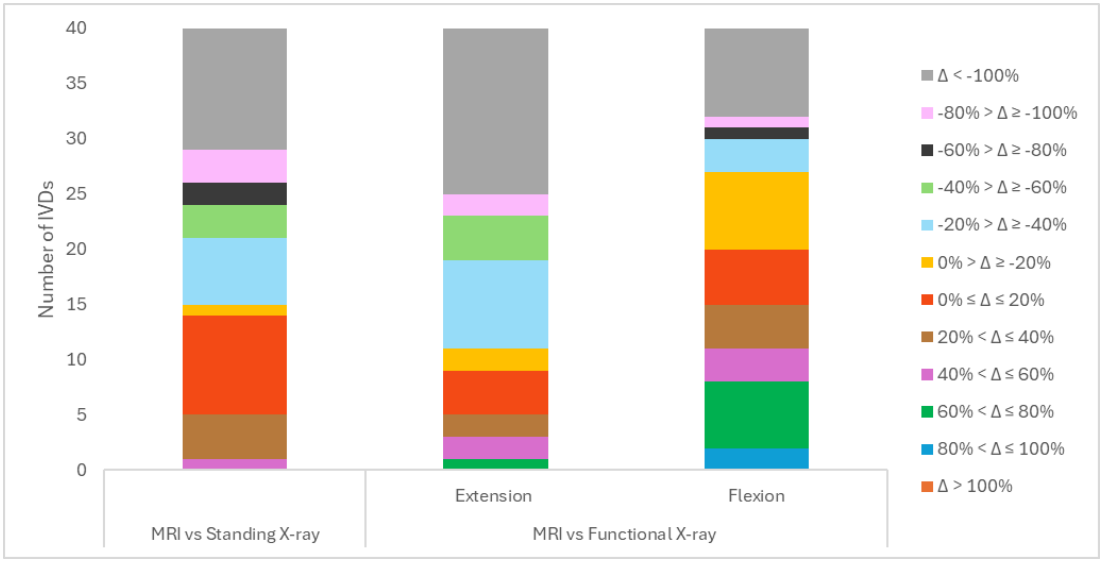

Figure 4.5 – Number of IVDs, for each percentage deviation interval, according to different combinations of imaging techniques, at intervertebral angle level (Group 1).

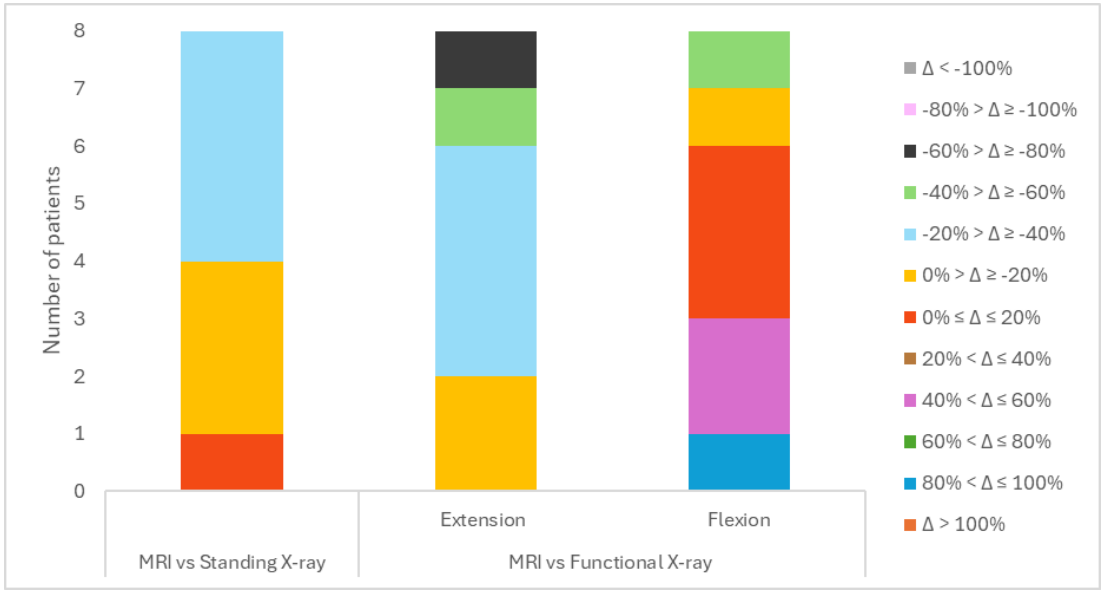

Figure 4.6 – Number of patients, for each percentage deviation interval, according to different combinations of imaging techniques, at lumbar lordosis angle level (Group 1).

In terms of the lumbar lordosis angle, and considering Figure 4.6, it was observed that Standing X-ray showed good agreement with MRI, as a large portion of the patients were in the -20% > Δ ≥ -40% and 0% > Δ ≥ -20% intervals. On the other hand, there were greater differences between MRI and Functional X-ray, especially in flexion, where some patients exhibited significant positive deviations. In extension, the measurements seemed to be more uniform, with smaller variations. This indicates that in flexion, Functional X-ray tends to show much lower lumbar lordosis angles than MRI. This analysis are aligned with the literature [51], as the lumbar lordosis angle tends to decrease when comparing MRI with Functional X-ray during flexion, while it tends to increase during extension.

4.5.3.2 Group 2

Figure 4.7 shows the number of IVDs, at IVD height level, for each percentage deviation interval, according to the diferrent combinations of imaging techniques.

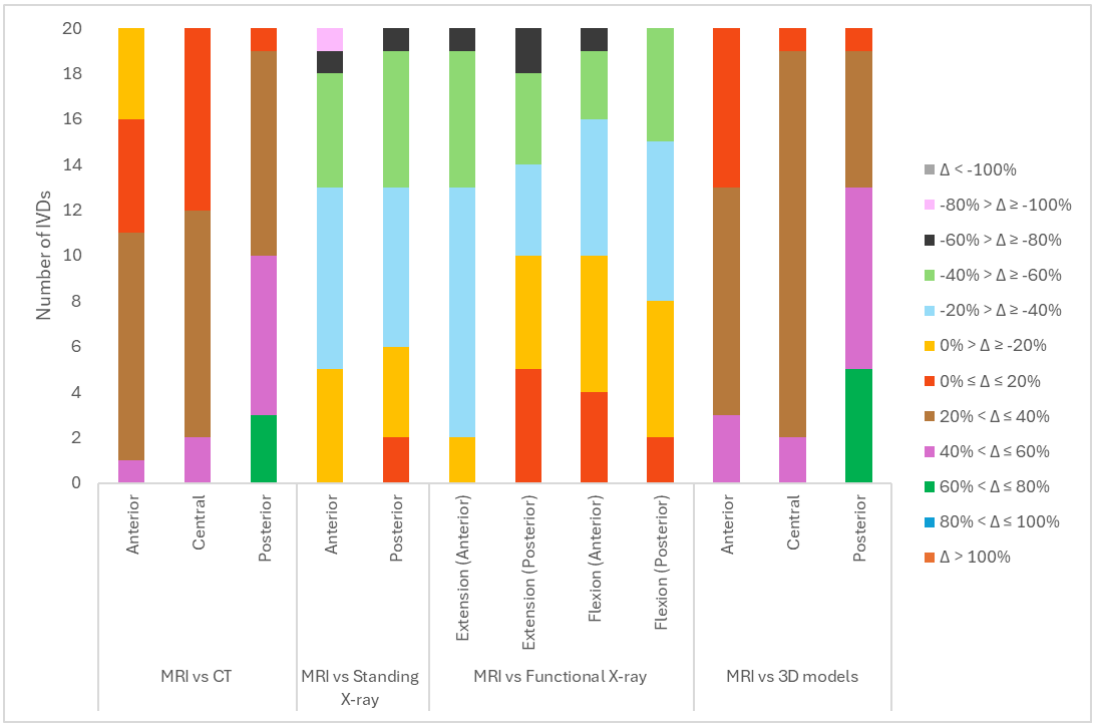

Figure 4.7 – Number of IVDs, for each percentage deviation interval, according to different combinations of imaging techniques, at IVD height level (Group 2).

Through the analysis of IVD height (Figure 4.7), it was observed that there was a greater agreement between MRI and CT, as well as between MRI and 3D models, which was expected, since most IVDs showed percentage deviations in the lower intervals ($0\% \leq \Delta \leq 20\%$ and $20\% < \Delta \leq 40\%$). Nevertheless, MRI tends to overestimate IVD height compared to CT and 3D models. The greatest discrepancies occurred when comparing MRI with Standing and Functional X-ray, as there was a significant number of IVDs in the $-40\% > \Delta \geq -60\%$ and $-60\% > \Delta \geq -80\%$ intervals, indicating that measurements in standing and dynamic imaging techniques are difficult to agree with MRI measurements. In relation to Standing X-ray and Functional X-ray, MRI generally underestimates IVD height. Furthermore, Group 2 seem inconsistent with the literature [49], as the IVDs showed greater heights in Standing and Functional X-ray compared to MRI.

Figure 4.8 shows the distribution of the number of vertebrae according to the vertebral height parameter.

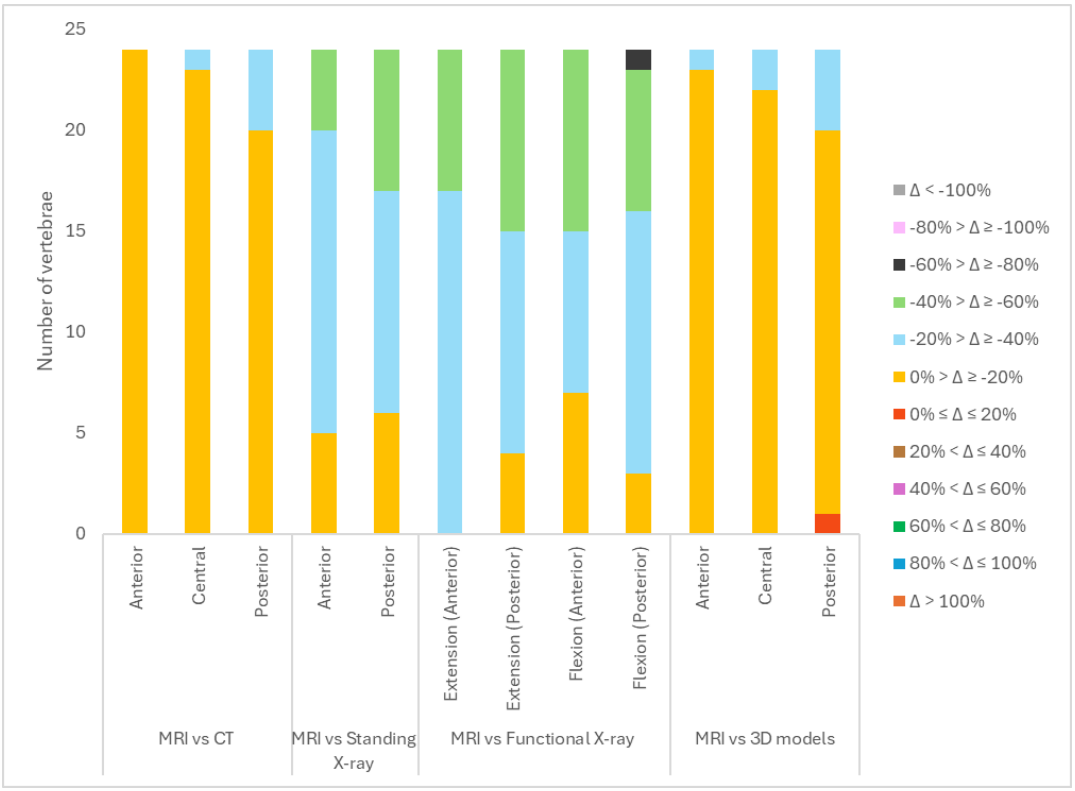

Figure 4.8 – Number of vertebrae, for each percentage deviation interval, according to different combinations of imaging techniques, at vertebral height level (Group 2).

It was observed that in CT and 3D models, most of the vertebrae were in the 0% > Δ ≥ -20% interval, indicating good agreement between CT and 3D models with MRI, which is supposed since the 3D models are based on CT scans. When comparing Standing and Functional X-ray with MRI, most values were in the -20% > Δ ≥ -40% interval, although there were a significant number of vertebrae in the -40% > Δ ≥ -60% interval. Therefore, it was concluded that Standing and Functional X-ray showed more discrepant values to MRI compared to CT and 3D models. However, this parameter exhibited lower percentage deviations variations compared to IVD height, as also observed in Group 1.

In terms of the intervertebral angle (Figure 4.9), the imaging modality with the best correspondence with MRI, in terms of the number of IVDs, was CT and the associated 3D models, as most IVDs exhibited small variations (0% > Δ ≥ -20%). However, the second interval with the highest number of IVDs corresponded to Δ < -100%, indicating that most of the IVDs had values that were either close to MRI or completely discrepant. As in Group 1, in Group 2 Standing and Functional X-ray (in both extension and flexion) showed significant discrepancies when compared to MRI, with differences in many percentage deviations intervals, which suggests that these modalities have significantly lower accuracy when compared to MRI.

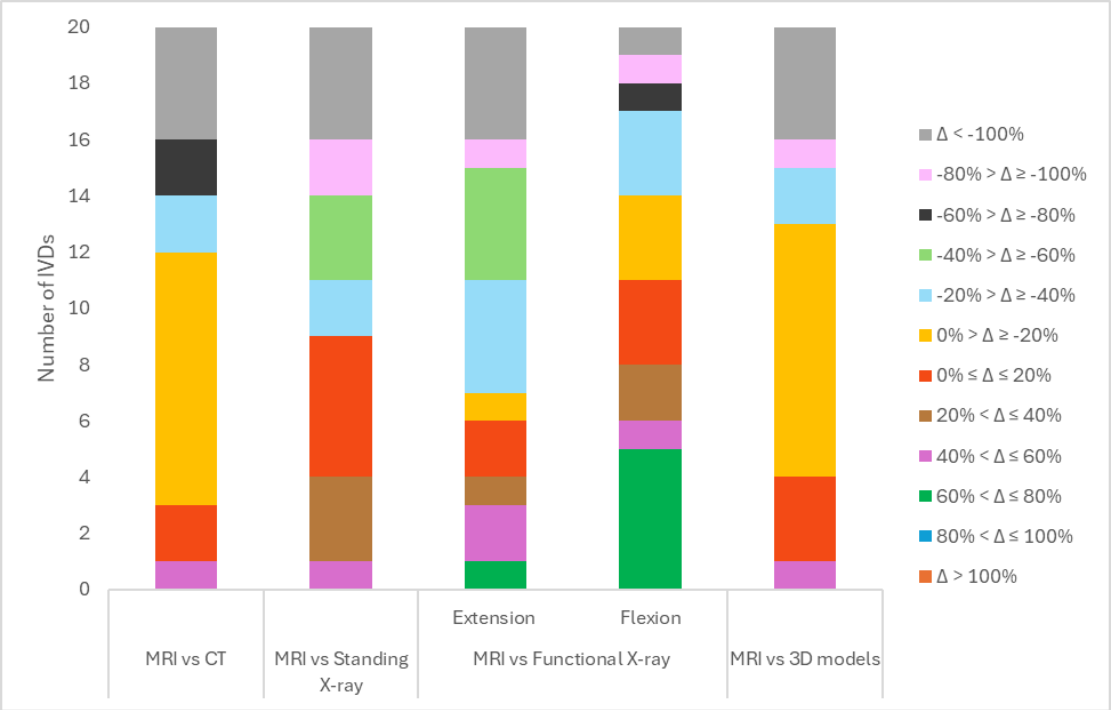

Figure 4.9 – Number of IVDs, for each percentage deviation interval, according to different combinations of imaging techniques, at intervertebral angle level (Group 2).

Regarding Figure 4.10, which corresponds to the lumbar lordosis angle, the imaging modality that showed the best correspondence with MRI, in terms of the number of patients, was CT and the 3D models, as most patients exhibited small variations (0% > Δ ≥ -20%). Standing X-ray also demonstrated good correspondence with MRI, with most patients within the -20% > Δ ≥ -40% interval. Finally, the Functional X-ray in flexion presented 2 patients with percentage deviation exceeding 40%, which was the most discrepant result compared to the other imaging techniques combinations. However, since the lumbar lordosis angle tends to decrease in flexion relative to MRI and increase in extension, the Functional X-ray outputs seem to align with the literature [51].

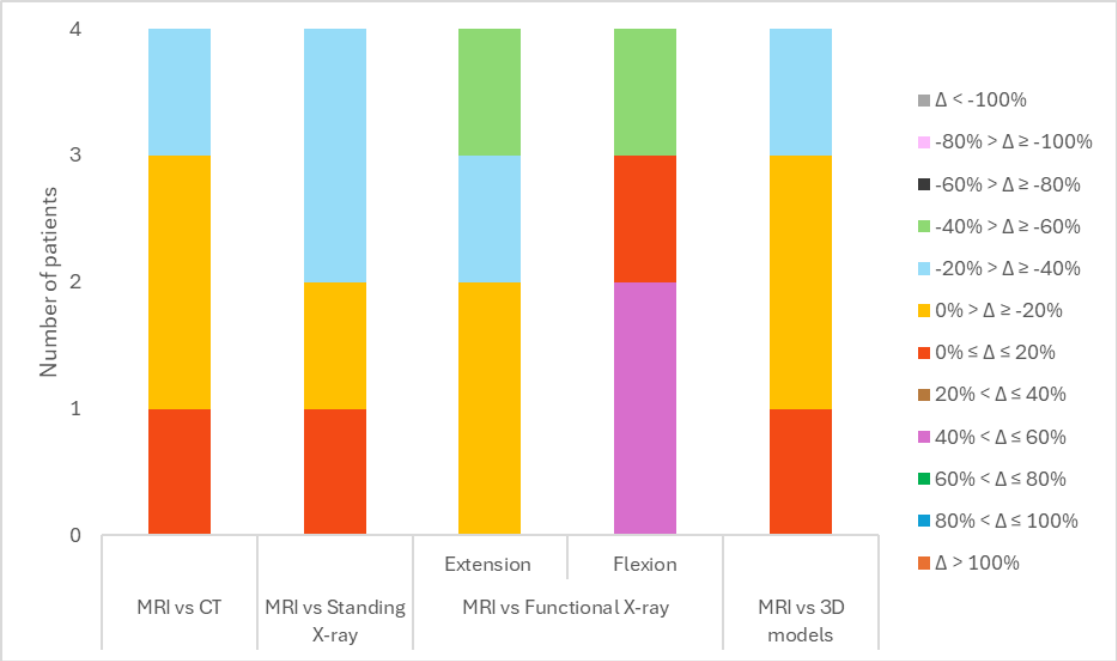

Figure 4.10 – Number of patients, for each percentage deviation interval, according to different combinations of imaging techniques, at lumbar lordosis angle level (Group 2).

4.5.3.3 Comparison between Group 1 and Group 2

From an analysis of the results obtained in both groups, it can be seen that for IVD height, in both Group 1 and Group 2, at Standing and Functional X-ray level, the percentage deviation interval with the highest number of IVDs corresponded to -20% > Δ ≥ -40%. This result implies that the IVD height measured in MRI tends to be lower than the IVD height measured in the X-rays exams. In Group 2, it can be seen that the IVD height in CT and 3D models, when

compared to MRI, was quite similar, since the percentage deviation intervals with the highest number of IVDs were $0\% \leq \Delta \leq 20\%$ and $20\% < \Delta \leq 40\%$.

Regarding vertebral height, when comparing Standing and Functional X-ray with MRI, in both groups, the vast majority of vertebrae were found to be in the $-20\% > \Delta \geq -40\%$ interval. However, in CT and 3D models, the vast majority of vertebrae were present in the $0\% > \Delta \geq -20\%$ interval. This parameter therefore shows the best agreement of all the imaging modalities, since the vast majority of vertebrae were found in the lower percentage deviation intervals and were concentrated in just 4 intervals.

In terms of intervertebral angle, this was the parameter with the greatest difference between the various imaging modalities, representing disagreement between the various exams. In both groups, both in Standing and Functional X-ray, the number of IVDs was widely dispersed in various percentage deviation intervals (-100% to 80%), with the $\Delta < -100\%$ interval showing a significant number of IVDs. On the other hand, in CT and 3D models, the interval with the highest number of IVDs concerned $0\% > \Delta \geq -20\%$, however, the second interval corresponded to $\Delta < -100\%$, which means that most of the IVDs present values close to MRI as completely discrepant values.

Finally, for the lumbar lordosis angle, in both Group 1 and Group 2, there was a good agreement between MRI and Standing X-ray, as the percentage deviation range with the highest number of patients was $-20\% > \Delta \geq -40\%$. On the other hand, for Functional X-ray, the percentage deviation ranges for extension movement were less than 0, while for flexion movement it were greater than 0. These results validate the biomechanical movement of the spine. In terms of CT and 3D models, the percentage deviation interval with the highest number of patients corresponded to $0\% > \Delta \geq -20\%$, which proves the good agreement between CT and 3D models with MRI.

5. Conclusions and Future Work

5.1 Conclusions

This study aimed to contribute to a better understanding of specific LBP, as well as to enhance the assessment and treatment of LDH that cause LBP, significantly impacting the quality of life of many individuals. In this regard, the objective of this study was to correlate clinical characteristics, quantitative and qualitative parameters from various imaging modalities and quantitative parameters from 3D models, in patients with LDH manifested as acute sciatica.

In general, the outputs indicated that clinical characteristics such as sex, age, BMI, functional impact (ODI) and pain intensity (NPRS) did not show a clear correlation with LDH area. Regarding quantitative parameters, measures obtained through Standing and Functional X-ray differed from those obtained using MRI and CT, due to variations in posture during image acquisition. It is important to note that Standing X-ray is often more representative of the actual load applied to the spine. Furthermore, through the combinations of imaging techniques and considering the evaluated parameters, it was concluded that MRI and CT (plus the associated 3D models) were the most similar to each other.

Regarding IVD height, the outputs of MRI versus Standing X-ray and MRI versus Functional X-ray were not aligned with the literature, while the combinations of MRI versus CT and MRI versus 3D models seemed to be in accordance with what was theoretically expected. For vertebral height, MRI demonstrated a relatively close correspondence with all the imaging modalities studied and 3D models, since most of the deviations were in relatively low percentage deviations intervals. The intervertebral angle showed the least agreement between 2 techniques, particularly in MRI versus Standing X-ray and MRI versus Functional X-ray, as it presented a significant number of IVDs in the maximum negative percentage deviation interval. The outputs for the lumbar lordosis angle were mostly in accordance with the literature.

This study provided a deeper understanding of the lumbar spine anatomy, the clinical procedures performed on patients with LDH, as well as the analysis and interpretation of imaging modalities. Additionally, the correlation between the quantitative parameters derived from imaging modalities and clinical parameters proved to be challenging. This complexity suggests the need for further investigation into the relation between quantitative, clinical and imaging parameters.

5.2 Limitations and Future Work

The main limitations of this study were associated with the small number of patients. Consequently, the analysis was conducted with a limited sample size (10 patients), which limited the establishment of significant correlations. A larger sample size is necessary to confirm the outputs obtained and to identify clearer, more precise patterns. Regarding the reliability of the outputs, it would be beneficial to have 2 more observers taking the measurements at the same time as the first observer, to establish intra-observer and inter-observer relations. Finally, concerning the imaging techniques, it was noted that few patients have a CT scan, possibly due to concerns about radiation exposure, which impacts on the number of 3D models available.

In conclusion, to mitigate the limitations of the study, several directions for future research can be considered. As far as 3D models are concerned, these could be developed from Standing X-ray examinations (or more advanced imaging modalities as the EOS [52]), as pain usually manifests when the patient is standing, and the only examination performed in that neutral position is Standing X-ray. Given that parametric 3D models of the lumbar spine already exist, which use cylindric shapes to represent the vertebrae, it would be possible to simulate the movements of the lumbar spine using the finite element method based on these representations and measurements obtained from Standing X-ray.

It would be interesting to carry out a biomechanical analysis of the gait pattern of the patients included in this study and relate the parameters extracted from this analysis to the clinical and imaging data. It would also be worthwhile to investigate the correlation between the EQ-5D-3L questionnaire and clinical and imaging parameters, as it is believed that pain sensitivity may be related to psychological conditions, such as anxiety or depression.

Finally, it is essential to increase the number of patients in the developed database in order to establish more robust relations between the various parameters. In addition, including healthy patients without lumbar spine pathology or pain, would enable a comparison between the clinical and imaging outputs obtained from patients with LDH and those without pathological changes in the same clinical setting, instead of relying in data from other datasets from healthy patients.

References

[1] I. Urits *et al.*, “Low Back Pain, a Comprehensive Review: Pathophysiology, Diagnosis, and Treatment,” *Curr. Pain Headache Rep.*, vol. 23, no. 3, pp. 1–10, 2019, doi: 10.1007/s11916-019-0757-1.

[2] P. Suri, J. Rainville, D. J. Hunter, L. Li, and J. N. Katz, “Recurrence of radicular pain or back pain after nonsurgical treatment of symptomatic lumbar disk herniation,” *Arch. Phys. Med. Rehabil.*, vol. 93, no. 4, pp. 690–695, 2012, doi: 10.1016/j.apmr.2011.11.028.

[3] L. Vialle, E. Vialle, J. Henao, and G. Giraldo, “Lumbar Disc Herniation,” *Rev. Bras. Ortop. (English Ed.*, vol. 45, no. 1, pp. 17–22, 2010, doi: 10.1007/s12178-017-9441-4.

[4] P. Natarajan, R. D. Fonseka, L. W. Sy, M. M. Maharaj, and R. J. Mobbs, “Analysing Gait Patterns in Degenerative Lumbar Spine Disease Using Inertial Wearable Sensors: An Observational Study,” *World Neurosurg.*, vol. 163, pp. e501–e515, 2022, doi: 10.1016/j.wneu.2022.04.013.

[5] K. Lee, E. S. Kim, B. Jung, S. W. Park, and I. H. Ha, “Association between pain and gait instability in patients with lumbar disc herniation,” *J. Int. Med. Res.*, vol. 49, no. 8, pp. 1–9, 2021, doi: 10.1177/03000605211039386.

[6] D. Davis, K. Maini, T. Muhammad, and A. Vasudevan, *StatPearls - Sciatica*. 2024.

[7] C. Liu *et al.*, “Surgical versus non-surgical treatment for sciatica: systematic review and meta-analysis of randomised controlled trials,” *BMJ*, vol. 381, pp. 1–14, 2023, doi: 10.1136/bmj-2022-070730.

[8] D. Chen *et al.*, “Three-dimensional reconstructions in spine and screw trajectory simulation on 3D digital images: a step by step approach by using Mimics software,” *J. Spine Surg.*, vol. 3, no. 4, pp. 650–656, 2017, doi: 10.21037/jss.2017.10.09.

[9] B. Sassack and J. D. Carrier, *StatPearls - Anatomy, Back, Lumbar Spine*. 2023.

[10] B. A. Frost, S. Camarero-Espinosa, and E. Johan Foster, “Materials for the spine: Anatomy, problems, and solutions,” *Materials (Basel).*, vol. 12, no. 2, pp. 1–41, 2019, doi: 10.3390/ma12020253.

[11] F. H. Netter, *Atlas de Anatomia Humana*. 2003.

[12] V. Mahadevan, “Anatomy of the vertebral column,” *Surg.*, vol. 36, no. 7, pp. 327–332, 2018, doi: 10.1016/j.mpsur.2018.05.006.

[13] M. Krismer and M. van Tulder, “Low back pain (non-specific),” *Best Pract. Res. Clin.*

Rheumatol., vol. 21, no. 1, pp. 77–91, 2007, doi: 10.1016/j.berh.2006.08.004.

[14] F. J. Lyu *et al.*, “Painful intervertebral disc degeneration and inflammation: from laboratory evidence to clinical interventions,” *Bone Res.*, vol. 9, no. 1, p. 14, 2021, doi: 10.1038/s41413-020-00125-x.

[15] M. J. Hancock, C. G. Maher, M. Laslett, E. Hay, and B. Koes, “Discussion paper: What happened to the bio in the bio-psycho-social model of low back pain?,” *Eur. Spine J.*, vol. 20, no. 12, pp. 2105–2110, 2011, doi: 10.1007/s00586-011-1886-3.

[16] B. W. Koes, “Improving the management of sciatica,” *Lancet Rheumatol.*, vol. 2, no. 7, p. 2, 2020, doi: 10.1016/S2665-9913(20)30130-2.

[17] R. Clark, R. P. Weber, and L. Kahwati, *Surgical Management of Lumbar Radiculopathy: a Systematic Review*, vol. 35, no. 3. Journal of General Internal Medicine, 2020, pp. 855–864.

[18] M. Fairag *et al.*, “Risk Factors, Prevention, and Primary and Secondary Management of Sciatica: An Updated Overview,” *Cureus*, vol. 14, no. 11, pp. 12–17, 2022, doi: 10.7759/cureus.31405.

[19] A. B. Schmid, L. Dove, L. Ridgway, and C. Price, *Early surgery for sciatica*. 2023.

[20] K. Koivunen, K. I. Pernaa, and M. Saltychev, “Back pain and radicular pain after lumbar microdiscectomy,” *BMC Surg.*, vol. 23, no. 1, pp. 1–9, 2023, doi: 10.1186/s12893-023-02114-3.

[21] D. F. Fardon, A. L. Williams, E. J. Dohring, F. R. Murtagh, S. L. Gabriel Rothman, and G. K. Sze, “Lumbar disc nomenclature: Version 2.0,” *Spine J.*, vol. 14, no. 11, pp. 2525–2545, 2014, doi: 10.1016/j.spinee.2014.04.022.

[22] “Disc Sequestration,” *Spine Clinic*, 2024. https://www.qispine.com/disc-sequestration-symptoms-causes-treatment.

[23] C. A. Benech, “Ernie discali,” 2024. https://www.benech-neurochirurgia.it/campi-dazione/ernie-discali/.

[24] A. J. Teichtahl, D. M. Urquhart, Y. Wang, A. E. Wluka, S. Heritier, and F. M. Cicuttini, “A Dose-response relationship between severity of disc degeneration and intervertebral disc height in the lumbosacral spine,” *Arthritis Res. Ther.*, vol. 17, no. 1, pp. 4–9, 2015, doi: 10.1186/s13075-015-0820-1.

[25] R. Compte *et al.*, “Are current machine learning applications comparable to radiologist classification of degenerate and herniated discs and Modic change? A systematic

review and meta-analysis," *Eur. Spine J.*, vol. 32, no. 11, pp. 3764–3787, 2023, doi: 10.1007/s00586-023-07718-0.

[26] J. Pesonen *et al.*, "Extending the straight leg raise test for improved clinical evaluation of sciatica: validity and diagnostic performance with reference to the magnetic resonance imaging," *BMC Musculoskelet. Disord.*, vol. 22, no. 1, pp. 1–9, 2021, doi: 10.1186/s12891-021-04781-w.

[27] S. N. Divi *et al.*, "Can imaging characteristics on magnetic resonance imaging predict the acuity of a lumbar disc herniation?," *Int. J. Spine Surg.*, vol. 15, no. 3, pp. 458–465, 2021, doi: 10.14444/8032.

[28] W. S. Bartynski and L. Lin, "Lumbar root compression in the lateral recess: MR imaging, conventional myelography, and CT myelography comparison with surgical confirmation," *Am. J. Neuroradiol.*, vol. 24, no. 3, pp. 348–360, 2003.

[29] M. A. Baker and S. MacKay, "Please be upstanding – A narrative review of evidence comparing upright to supine lumbar spine MRI," *Radiography*, vol. 27, no. 2, pp. 721–726, 2021, doi: 10.1016/j.radi.2020.11.003.

[30] A. Ribeiro, "Manual de Tomografia Computorizada do Técnico de Imagiologia Médica," 2007.

[31] G.-L. Wong and Wing-Tak, "Magnetic Resonance Imaging (MRI)," *Natl. Inst. Biomed. Imaging Bioeng.*, pp. 11–14, 2022.

[32] N. Smith and A. Webb, *Introduction to Medical Imaging: Physics, Engineering and Clinical Aplications*. 2010.

[33] X. Ou *et al.*, "Recent Development in X-Ray Imaging Technology: Future and Challenges," *Research*, p. 18, 2021, doi: 10.34133/2021/9892152.

[34] J. DVOŘÁK, M. PANJABI, D. CHANG, R. THEILER, and D. GROB, "Functional Radiographic Diagnosis of the Lumbar Spine," *Physiol. Behav.*, vol. 16, no. 5, p. 562.571, 1991, doi: 10.1097/00007632-199105000-00014.

[35] M. Schulze, F. Trautwein, T. Vordemvenne, M. Raschke, and F. Heuer, "A method to perform spinal motion analysis from functional X-ray images," *J. Biomech.*, vol. 44, no. 9, pp. 1740–1746, 2011, doi: 10.1016/j.jbiomech.2011.03.040.

[36] K. Shah, M. Solan, and E. Dawe, "The gait cycle and its variations with disease and injury," *Orthop. Trauma*, vol. 34, no. 3, pp. 153–160, 2020, doi: 10.1016/j.mporth.2020.03.009.

[37] Y. P. Huang *et al.*, “Gait adaptations in low back pain patients with lumbar disc herniation: Trunk coordination and arm swing,” *Eur. Spine J.*, vol. 20, no. 3, pp. 491–499, 2011, doi: 10.1007/s00586-010-1639-8.

[38] P. Natarajan, R. D. Fonseka, S. Kim, C. Betteridge, M. Maharaj, and R. J. Mobbs, “Analysing gait patterns in degenerative lumbar spine diseases: a literature review,” *J. Spine Surg.*, vol. 8, no. 1, pp. 139–148, 2022, doi: 10.21037/jss-21-91.

[39] R. Matos, “Segmentação de discos intervertebrais lombares para modelação e simulação computacional,” 2021.

[40] M. B. Pernas, “Novo método de caracterização 3D da escoliose idiopática do adolescente,” 2023.

[41] S. Wang, Z. Jiang, H. Yang, X. Li, and Z. Yang, “MRI-Based Medical Image Recognition: Identification and Diagnosis of LDH,” *Comput. Intell. Neurosci.*, vol. 2022, p. 9, 2022, doi: 10.1155/2022/5207178.

[42] J. W. van der Graaf *et al.*, “Lumbar spine segmentation in MR images: a dataset and a public benchmark,” *Sci. Data*, vol. 11, no. 1, pp. 1–9, 2024, doi: 10.1038/s41597-024-03090-w.

[43] S. Waldman, *Pain Management (Second Edition)*. 2011.

[44] M. Yates and N. Shastri-Hurst, “The oswestry disability index,” *Occup. Med. (Chic. Ill).*, vol. 67, no. 3, pp. 241–242, 2017, doi: 10.1093/occmed/kqw051.

[45] İ. Malkoc *et al.*, “Age Related Changes in Height and Shape of the Lumbar İntervertebral Discus,” *Eur. J. Basic Med. Sci.*, vol. 2, no. 3, pp. 68–73, 2012, doi: 10.21601/ejbms/9182.

[46] C. Weir and A. Jan, *StatPearls - BMI Classification Percentile and Cut Off Points*. 2024.

[47] D. Samartzis, J. Karppinen, K. D. Luk, and K. M. Cheung, “Body Mass Index and its Association with Lumbar Disc Herniation and Sciatica: A Large-Scale, Population-Based Study,” *Glob. Spine J.*, vol. 4, no. 1, 2014, doi: 10.1055/s-0034-1376593.

[48] S. H. Vučković *et al.*, “Correlation of MRI Findings with ODI and VAS Score in Patients with Lower Back Pain,” *Open Neuroimag. J.*, vol. 16, p. 10, 2023, doi: 10.2174/18743129-v16-230911-2022-4.

[49] S. Son, S. G. Lee, W. K. Kim, Y. Ahn, and J. M. Jung, “Disc height discrepancy between supine and standing positions as a screening metric for discogenic back pain in

patients with disc degeneration," *Spine J.*, vol. 21, no. 1, pp. 71–79, 2021, doi: 10.1016/j.spinee.2020.07.006.

[50] T. Jentzsch, K. E. Mantel, K. Slankamenac, G. Osterhoff, and C. M. L. Werner, "CT-based surrogate parameters for MRI-based disc height and endplate degeneration in the lumbar spine," *BMC Med. Imaging*, vol. 24, no. 213, pp. 1–9, 2024, doi: 10.1186/s12880-024-01395-1.

[51] D. Viggiani, K. M. Gallagher, M. Sehl, and J. P. Callaghan, "The distribution of lumbar intervertebral angles in upright standing and extension is related to low back pain developed during standing," *Clin. Biomech.*, vol. 49, pp. 85–90, 2017, doi: 10.1016/j.clinbiomech.2017.09.003.

[52] B. Garg, N. Mehta, T. Bansal, and R. Malhotra, "EOS® imaging: Concept and current applications in spinal disorders," *J. Clin. Orthop. Trauma*, vol. 11, no. 5, pp. 786–793, 2020, doi: 10.1016/j.jcot.2020.06.012.

Appendices

Appendix 1 – Quantitative parameters measured in MRI.

Parameter name	Plane	Slice	Measurement units	Method	Example
IVD height	Sagittal	Column midline	mm	Anterior height – Anterior boundary between the two adjacent vertebrae (at the centre of the vertebral curvature) Central height – Boundary that starts at the lower midpoint of the IVD and ends at the upper midpoint of the IVD Posterior height – Posterior boundary between the two adjacent vertebrae (at the centre of the vertebral curvature)	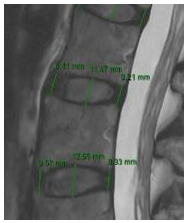
	Coronal	Cutting plane in the centre of the vertebrae/IVDs	mm	Left height – Left boundary between the two adjacent vertebrae (in the centre of the vertebral curvature) Central height – Boundary that starts at the lower midpoint of the IVD and ends at the upper midpoint of the IVD Right height – Right boundary between the two adjacent vertebrae (in the centre of the vertebral curvature)	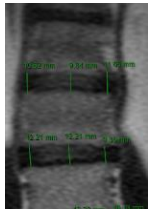
Vertebra height	Sagittal	Column midline	mm	Anterior height – Maximum anterior boundary between the curvatures of the vertebra (centre of the curvatures) Central height – Boundary that begins at the lower midpoint of the vertebra and ends at the upper midpoint of the vertebra Posterior height – Maximum posterior boundary between the curvatures of the vertebra (centre of the curvatures)	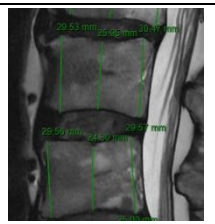
	Coronal	Cutting plane in the centre of the vertebrae/IVDs	mm	Left height – Left boundary between the curvatures of the vertebra (centre of the curvatures) Central height – Boundary that starts at the lower midpoint of the vertebra and ends at the upper midpoint of the vertebra Right height – Right boundary between the curvatures of the vertebra (centre of the curvatures)	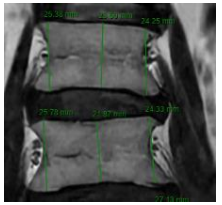

IVD length	Sagittal	Column midline	mm	Draw a line from the beginning of the IVD (anterior longitudinal ligament – midline) to its end (posterior longitudinal ligament – midline)	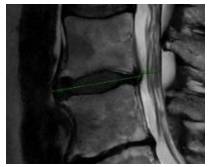
Intervertebral angle	Sagittal	Column midline	°	Draw a tangent line to the superior endplate of the lower vertebra and a tangent line to the inferior endplate of the upper vertebra	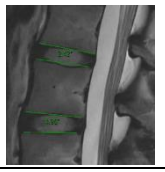
	Coronal	Cutting plane in the centre of the vertebrae/IVDs			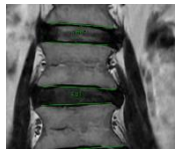
Lumbar lordosis angle	Sagittal	Column midline	°	Draw a tangent line to the superior endplate of the L1 vertebra and a tangent line to the superior endplate of the S1 vertebra	
Anteroposterior canal diameter at vertebra level	Sagittal	Column midline	mm	Measure the diameter of the canal horizontally (according to the inclination of each vertebra) at the level of the midline of the vertebra above and below the LDH	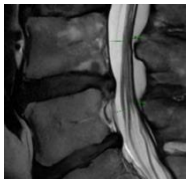
Anteroposterior canal diameter at IVD level	Sagittal	Column midline	mm	Measure the diameter of the canal horizontally (according to the inclination of each IVD) at the level of the midline of the IVD containing the LDH	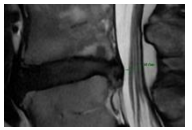

Greatest anteroposterior projection of the LDH	Axial	Axial plane containing the largest LDH	mm	Measure the antero-posterior distance, considering the inclination of the vertebra, from the posterior side (end of the herniated IVD boundary) to the anterior side (end of the IVD boundary) of the herniated IVD	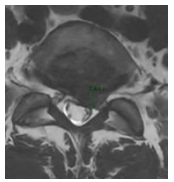
Centra signal	Sagittal	Sagittal plane containing the largest LDH	mm^2	Select the area of the IVD under analysis without the herniation, from the beginning of the IVD (anterior longitudinal ligament) to the anterior boundary of the herniation	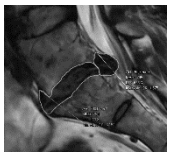
Herniation signal				Select the LDH area	
Canal area without LDH	Axial	Axial plane containing the largest LDH	mm^2	1. Measure the area of the entire vertebral canal, including the LDH (excluding fat) 2. Measure the area of the LDH present in the vertebral canal Calculate: Area of the canal with LDH – Area of the LDH	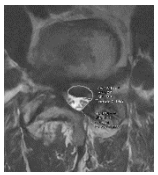
Foramen area (left and right)	Sagittal	External and internal limits of each foramen	mm^2	Measure the foramen area (excluding fat and ligaments) between the pedicles of the vertebrae, the inferior articular process of the superior vertebra, the superior articular process of the inferior vertebra and the intervertebral IVD	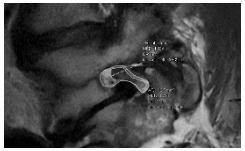
Root area (left and right)	Sagittal	External and internal limits of each foramen	mm^2	Measure the area of the nerve root present at the external and internal boundaries of each foramen	
Useful foramen area	Sagittal	-	mm^2	Calculate: Foramen area – Root area (for each boundary – external and internal and for each side – right and left)	-
Greater foramen diameter	Sagittal	Plane with the largest foramen area	mm	In the foramen with the largest area, measure the largest diameter of the foramen (diagonal/vertical)	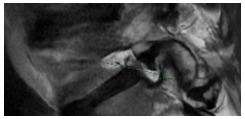
Greater root diameter	Sagittal	Plane with the largest root area	mm	In the root with the largest area, measure the greatest diameter of the root (diagonal/vertical)	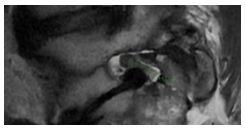

Appendix 2 – Clinical parameters.

Socio-demographic and LDH data											
HLS	**Age (years)**	**Sex**	**Height (m)**	**Weight (kg)**	**BMI (kg/m^2)**	**BMI Classification**	**Treatment Group**	**Dominant symptoms**	**Symptomatic levels**	**LDH level**	**Laterality**
HLS.053	56	M	1.71	85	29.1	Overweight	Surgical	Radicular pain	L5	L4-L5	Left
HLS.055	49	F	1.56	63	25.9	Overweight	Surgical	Radicular pain	L5, S1	L5-S1	Left
HLS.056	50	M	1.82	125	37.7	Obesity Grade II	Surgical	Radicular pain + Lumbar pain	L5, S1	L4-L5 and L5-S1	Right + Left
HLS.062	67	F	1.67	85	30.5	Obesity Grade I	Conservative	Asymptomatic	S1	L4-L5 and L5-S1	Left
HLS.063	57	M	1.76	120	38.7	Obesity Grade II	Conservative	Radicular pain	L5, S1	L3-L4	Right
HLS.064	54	M	1.78	91	28.7	Overweight	Conservative	Radicular pain	L4, L5	L3-L4	Right
HLS.067	75	F	1.62	58	22.1	Normal Weight	Surgical	Radicular pain + Lumbar pain	L5	L2-L3	Right
HLS.070	59	F	1.70	115	39.8	Obesity Grade II	Surgical	Radicular pain + Lumbar pain	L4, L5	L3-L4, L4-L5 and L5-S1	Left
HLS.072	28	F	1.65	55	20.2	Normal Weight	Surgical	Radicular pain	L5, S1	L5-S1	Right
HLS.075	43	F	1.67	76	27.3	Overweight	Surgical	Radicular pain	S1	L5-S1	Left

NPRS data				
HLS	**NPRS Axial Basal**	**NPRS Axial Peak**	**NPRS Radicular Basal**	**NPRS Radicular Peak**
HLS.053	0	0	4	8
HLS.055	0	0	4	10
HLS.056	0	0	4	9
HLS.062	0	0	0	0
HLS.063	0	0	6	8
HLS.064	0	3	0	7
HLS.067	4	8	4	9
HLS.070	0	0	8	10
HLS.072	0	0	8	10
HLS.075	0	0	8	10

ODI data											
HLS	**Pain intensity**	**Personal care**	**Weight-lifting**	**Walking**	**Seating**	**Standing**	**Sleep**	**Sexual life**	**Social life**	**Travel**	**ODI total**
HLS.053	3	1	5	3	4	5	3	5	5	5	78
HLS.055	4	2	2	0	2	2	1	2	3	3	42
HLS.056	4	3	3	0	0	1	1	3	3	1	38
HLS.062	3	1	3	0	2	1	1	1	1	1	28
HLS.063	4	2	3	4	2	2	3	1	2	3	52
HLS.064	1	3	3	1	3	2	2	4	4	3	52
HLS.067	3	3	3	1	4	1	4	NA	3	3	50
HLS.070	4	2	4	3	2	4	2	NA	3	5	58
HLS.072	4	1	2	1	3	2	3	2	3	3	48
HLS.075	4	2	3	2	5	0	2	0	3	3	48

Appendix 3 – Average parameters measured in CT.

CT IVD height (mm)						
IVD	**Sagittal Plane**			**Coronal Plane**		
	Anterior	**Central**	**Posterior**	**Left**	**Central**	**Right**
L1-L2	7.42 ± 1.84	9.04 ± 1.01	3.05 ± 0.70	8.02 ± 1.32	8.09 ± 1.11	7.20 ± 1.51
L2-L3	8.08 ± 1.59	8.93 ± 1.68	3.97 ± 0.90	7.84 ± 0.80	8.37 ± 0.96	7.93 ± 1.22
L3-L4	10.60 ± 1.45	10.54 ± 0.95	4.89 ± 1.23	7.80 ± 1.63	9.86 ± 1.21	8.29 ± 0.46
L4-L5	11.43 ± 9.96	9.96 ± 2.46	5.11 ± 1.26	5.94 ± 1.23	9.85 ± 1.79	6.45 ± 1.71
L5-S1	9.11 ± 2.22	6.86 ± 1.26	4.81 ± 1.21	-	-	-

CT vertebral height (mm)						
Vertebra	**Sagittal Plane**			**Coronal Plane**		
	Anterior	**Central**	**Posterior**	**Left**	**Central**	**Right**
L1	27.21 ± 0.63	25.95 ± 2.19	31.05 ± 2.39	27.18 ± 0.92	26.10 ± 2.08	27.13 ± 0.99
L2	29.29 ± 0.90	25.89 ± 2.16	31.02 ± 1.61	28.06 ± 0.93	26.99 ± 2.14	28.35 ± 1.04
L3	30.10 ± 0.91	25.31 ± 1.61	29.78 ± 1.44	29.00 ± 1.42	26.62 ± 2.03	29.33 ± 1.06
L4	29.61 ± 0.45	26.60 ± 2.50	29.46 ± 1.68	31.02 ±1.41	26.49 ± 2.49	29.83 ± 1.12
L5	30.56 ± 1.15	24.78 ± 2.14	24.80 ± 1.13	28.64 ± 2.64	24.51 ± 2.86	28.61 ± 2.12
S1	32.46 ± 2.98	26.59 ± 3.36	26.08 ± 3.44	-	-	-

CT intervertebral angle (°)		
IVD	**Sagittal Plane**	**Coronal Plane**
L1-L2	8.11 ± 1.46	1.00 ± 0.18
L2-L3	8.71 ± 2.01	1.61 ± 1.60
L3-L4	8.86 ± 1.35	1.53 ± 1.39
L4-L5	10.00 ± 2.72	1.68 ± 1.52
L5-S1	9.04 ± 3.25	-

Appendix 4 – Average parameters measured in Standing X-ray.

Standing X-ray IVD height (mm)				
IVD	**Sagittal Plane**		**Coronal Plane**	
	Anterior	**Posterior**	**Left**	**Right**
L1-L2	12.30 ± 1.42	8.23 ± 2.13	6.43 ± 1.54	6.87 ± 1.85
L2-L3	13.67 ± 2.09	8.98 ± 1.75	8.18 ± 3.89	7.91 ± 3.69
L3-L4	16.48 ± 1.51	8.94 ± 2.11	8.90 ± 3.58	9.31 ± 2.89
L4-L5	15.91 ± 2.70	9.52 ± 1.75	8.82 ± 2.28	7.88 ± 2.88
L5-S1	15.34 ± 3.43	8.38 ± 2.02	-	-

Standing X-ray vertebral height (mm)				
Vertebra	**Sagittal Plane**		**Coronal Plane**	
	Anterior	**Posterior**	**Left**	**Right**
L1	33.35 ± 3.21	35.17 ± 2.88	27.87 ± 2.30	27.87 ± 2.87
L2	35.09 ± 3.48	36.43 ± 3.63	28.65 ± 2.34	28.36 ± 2.63
L3	36.66 ± 3.20	35.73 ± 2.61	30.87 ± 2.43	31.14 ± 2.90
L4	35.66 ± 2.96	33.67 ± 2.26	33.59 ± 1.69	33.17 ± 2.32
L5	37.93 ± 3.00	30.88 ± 1.72	35.54 ± 2.44	35.97 ± 2.34
S1	42.50 ± 4.46	34.93 ± 4.43	-	-

Standing X-ray intervertebral angle (°)	
IVD	**Sagittal Plane**
L1-L2	7.09 ± 2.26
L2-L3	7.78 ± 2.82
L3-L4	10.15 ± 2.86
L4-L5	10.54 ± 2.91
L5-S1	11.66 ± 6.39

Appendix 5 – Average parameters measured in Functional X-ray.

Functional X-ray IVD height (mm)				
IVD	**Extension**		**Flexion**	
	Anterior	**Posterior**	**Anterior**	**Posterior**
L1-L2	12.71 ± 1.38	7.75 ± 2.39	10.10 ± 2.04	9.03 ± 1.94
L2-L3	14.92 ± 1.39	8.51 ± 1.66	12.00 ± 2.02	9.69 ± 1.55
L3-L4	16.23 ± 1.58	8.89 ± 2.23	13.89 ± 2.55	9.59 ± 1.49
L4-L5	17.02 ± 1.85	9.75 ± 1.75	14.58 ± 2.59	9.63 ± 2.58
L5-S1	16.71 ± 3.59	8.06 ± 1.87	14.61 ± 2.57	8.59 ± 1.52

Functional X-ray vertebral height (mm)				
Vertebra	**Extension**		**Flexion**	
	Anterior	**Posterior**	**Anterior**	**Posterior**
L1	33.52 ± 3.26	35.68 ± 4.09	34.31 ± 3.32	35.31 ± 3.08
L2	35.12 ± 3.72	36.89 ± 3.45	36.21 ± 3.51	36.67 ± 3.09
L3	36.61 ± 2.99	35.80 ± 2.77	35.66 ± 3.78	36.50 ± 2.58
L4	35.87 ± 2.91	33.11 ± 1.40	35.65 ± 3.61	34.72 ± 3.06
L5	38.02 ± 3.01	31.16 ± 1.61	37.52 ± 2.55	30.93 ± 1.41
S1	44.62 ± 2.57	37.00 ± 5.00	40.38 ± 4.40	33.46 ± 4.22

Functional X-ray intervertebral angle (°)		
IVD	**Extension**	**Flexion**
L1-L2	7.79 ± 2.85	3.96 ± 2.81
L2-L3	8.91 ± 2.67	4.44 ± 3.06
L3-L4	10.29 ± 3.36	6.64 ± 3.72
L4-L5	12.15 ± 3.90	7.08 ± 3.99
L5-S1	15.22 ± 6.60	9.51 ± 4.98

Appendix 6 – Average parameters measured in 3D models.

3D model IVD height (mm)						
IVD	**Sagittal Plane**			**Coronal Plane**		
	Anterior	**Central**	**Posterior**	**Left**	**Central**	**Right**
L1-L2	6.90 ± 1.59	7.98 ± 0.60	2.85 ± 0.67	6.81 ± 0.89	7.73 ± 0.86	6.63 ± 1.36
L2-L3	7.64 ± 1.56	7.80 ± 1.91	3.99 ± 1.10	6.77 ± 0.19	7.48 ± 1.44	6.96 ± 0.70
L3-L4	9.69 ± 1.00	9.36 ± 1.28	4.21 ± 1.54	6.64 ± 1.92	9.50 ± 0.74	7.58 ± 1.09
L4-L5	10.73 ± 2.20	9.36 ± 1.35	4.33 ± 1.15	5.67 ± 1.05	8.67 ± 1.35	6.20 ± 1.13
L5-S1	8.52 ± 2.08	5.96 ± 0.77	4.20 ± 1.25	-	-	-

3D model vertebral height (mm)						
Vertebra	**Sagittal Plane**			**Coronal Plane**		
	Anterior	**Central**	**Posterior**	**Left**	**Central**	**Right**
L1	27.61 ± 0.80	26.42 ± 1.93	31.08 ± 2.74	28.34 ± 0.89	26.40 ± 1.91	28.03 ± 1.69
L2	29.73 ± 1.21	27.22 ± 2.19	31.11 ± 1.75	28.68 ± 1.23	26.67 ± 2.01	28.70 ± 1.42
L3	30.56 ± 0.46	26.55 ± 1.52	30.09 ± 1.34	29.18 ± 1.43	26.15 ± 1.52	29.71 ± 1.06
L4	30.60 ± 0.26	26.98 ± 1.36	29.85 ± 1.92	30.64 ± 1.25	26.47 ± 1.82	30.35 ± 1.01
L5	31.70 ± 0.92	25.79 ± 2.15	25.78 ± 0.96	29.40 ± 1.60	25.91 ± 1.73	28.83 ± 2.84
S1	33.15 ± 3.18	27.79 ± 3.33	26.49 ± 3.25	-	-	-

3D model intervertebral angle (°)		
IVD	**Sagittal Plane**	**Coronal Plane**
L1-L2	7.30 ± 1.67	1.24 ± 0.21
L2-L3	8.47 ± 2.04	1.76 ± 1.64
L3-L4	8.90 ± 1.25	1.62 ± 1.39
L4-L5	9.86 ± 2.41	1.84 ± 1.65
L5-S1	9.22 ± 3.89	-

Appendix 7 – Average anterior (A) and posterior (P) heights of each IVD (mm) in each patient in the study.

	L1-L2		L2-L3		L3-L4	
	A	**P**	**A**	**P**	**A**	**P**
HLS.053	11.62 ± 0.09	6.76 ± 0.07	12.06 ± 0.53	7.42 ± 0.27	13.44 ± 0.14	8.89 ± 0.23
HLS.055	7.24 ± 0.27	7.53 ± 0.31	9.70 ± 0.91	7.94 ± 0.20	8.98 ± 0.42	8.53 ± 0.15
HLS.056	10.61 ± 0.07	5.52 ± 0.47	12.18 ± 0.63	7.57 ± 0.31	12.40 ± 0.62	7.78 ± 0.28
HLS.062	9.33 ± 0.31	9.63 ± 0.31	10.08 ± 0.34	8.84 ± 0.12	12.08 ± 0.30	8.35 ± 0.28
HLS.063	8.60 ± 0.44	6.03 ± 0.16	10.92 ± 0.29	7.74 ± 0.32	12.87 ± 0.30	8.12 ± 0.33
HLS.064	8.09 ± 0.35	6.17 ± 0.44	9.45 ± 0.20	6.13 ± 0.09	12.19 ± 0.18	7.36 ± 0.18
HLS.067	11.82 ± 0.22	8.93 ± 0.10	11.87 ± 0.48	7.72 ± 0.51	9.74 ± 0.49	5.94 ± 0.58
HLS.070	9.27 ± 0.33	7.01 ± 0.31	7.06 ± 0.20	4.80 ± 0.09	12.36 ± 0.12	8.58 ± 0.21
HLS.072	6.64 ± 0.44	6.73 ± 0.00	8.08 ± 0.31	7.51 ± 0.21	10.49 ± 0.23	8.71 ± 0.33
HLS.075	8.90 ± 0.08	8.18 ± 0.07	9.94 ± 0.16	9.21 ± 0.11	12.70 ± 0.14	9.23 ± 0.27

	L4-L5		L5-S1	
	A	**P**	**A**	**P**
HLS.053	13.55 ± 0.62	7.70 ± 0.24	11.41 ± 0.85	7.07 ± 0.21
HLS.055	13.99 ± 0.23	9.83 ± 0.20	8.36 ± 0.20	6.52 ± 0.20
HLS.056	11.49 ± 0.19	5.58 ± 0.16	11.04 ± 0.82	7.22 ± 0.13
HLS.062	12.87 ± 0.31	6.34 ± 0.24	14.28 ± 0.20	6.67 ± 0.70
HLS.063	16.68 ± 0.24	8.37 ± 0.43	16.53 ± 0.36	8.22 ± 0.54
HLS.064	8.15 ± 0.70	4.06 ± 0.37	9.33 ± 0.36	6.11 ± 0.07
HLS.067	15.43 ± 0.07	8.19 ± 0.27	14.41 ± 0.19	7.41 ± 0.19
HLS.070	9.20 ± 0.42	8.35 ± 0.25	11.23 ± 0.17	5.11 ± 0.20
HLS.072	13.60 ± 0.19	8.48 ± 0.57	14.97 ± 0.46	6.28 ± 0.75
HLS.075	13.76 ± 0.04	8.02 ± 0.29	11.93 ± 0.37	8.34 ± 0.20

Appendix 8 – Tables 1 and 2 of Article "Age Related Changes in Height and Shape of The Lumbar Intervertebral Discus" [45].

***Table 1**. Changes of anterior height of the lumbar intervertebral discs of both sexes (mm) by age groups (decades). F=female, M=male. The varied lower case in the decades indicates the differences between the age groups (a, b, c →).*

	Sex	DECADES						
		10-19	20-29	30-39	40-49	50-59	60-69	70-79
		Mean±SD	Mean±SD	Mean±SD	Mean±SD	Mean±SD	Mean±SD	Mean±SD
L1	F	7.94±1.75^{b}	8.56±1.08$^{\#ab}$	9.04±1,2$^{\#ab}$	9.76±1.14^{a}	9.64±.93^{a}	9.59±1,33^{a}	9.6±1.58^{a}
	M	9.68±1.17^{b}	9.83±1.61^{b}	9.89±.96^{b}	9.92±1.15^{b}	10.53±1.5^{ab}	10.16±1.1^{b}	11.46±1.9^{a}
L2	F	8.81±2.26^{b}	10.28±1.3^{ab}	10.4±1,5$^{\#ab}$	11.21±1.6^{a}	11.21±1,19^{a}	10.8±2.2^{a}	10.61±2.5^{a}
	M	10.97±1.5^{a}	11.47±2.6^{a}	11.84±1.3^{a}	11.19±1.5^{a}	10.95±1.15^{a}	11.59±1.6^{a}	12.28±1.2^{a}
L3	F	9.95±2.6^{b}	11.59±1.3^{ab}	12.35±1.19^{a}	12.49±1.51^{a}	12.45±2.22^{a}	11.57±1.8^{ab}	12.24±2.05^{a}
	M	11.66±2.14^{b}	12.41±2.42^{ab}	12.86 ±1.85^{ab}	12.79±1.93^{ab}	12.34±2.08^{ab}	12.55±1.88^{ab}	14.06±2.35^{a}
L4	F	13.33±2.97^{a}	13.6±1.36^{a}	13.49±1.99^{a}	14.09±2.01^{a}	14.80±2.27^{a}	13.72±2.41^{a}	14.53±3.35^{a}
	M	12.98±1.97^{a}	14.33±2.06^{a}	13.84±1.66^{a}	14.44±1.67^{a}	14.29 ±2.59^{a}	13.21 ±3.23^{a}	14.47±1.79^{a}
L5	F	13.55±3.24^{a}	14.45±1.6^{a}	13.74±3.96^{a}	14.38 ±3.18^{a}	16.6±3.39^{a}	15.01 ±4.32^{a}	14.4±4.82^{a}
	M	13.06±1.62^{b}	13.92±3.53^{ab}	14.17±3.32^{ab}	16.58±2.89^{a}	14.75±2.93^{ab}	16.13±3.08^{a}	16.39±4.46^{a}

: male> female is significant (p<0.05)

***Table 2**. Changes of posterior height of the lumbar intervertebral discs of both sexes (mm) by age groups (decades). F=female, M=male. The varied lower case in the decades indicates the differences between the age groups (a, b, c →).*

	Sex	DECADES						
		10-19	20-29	30-39	40-49	50-59	60-69	70-79
		Mean±SD	Mean±SD	Mean±SD	Mean±SD	Mean±SD	Mean±SD	Mean±SD
L1	F	6.48 ±2.52^{a}	7.1 ±1.32^{a}	6.99 ±1.06^{a}	6.91±1.06^{a}	7.19±1.08^{a}	7.1±1.68^{a}	6.94±2.01^{a}
	M	7.39±1.1^{a}	6.94±1.41^{a}	6.89±1.65^{a}	6.82±1.24^{a}	6.58±1.11^{a}	6.48±0.67^{a}	6.8±1.4^{a}
L2	F	6.98±2.22^{a}	7.67±1.12^{a}	7.37±0.63^{a}	7.78±1.04^{a}	7.91±1.07^{a}	7.45±1.56^{a}	7.41±1.11^{a}
	M	8.28±0.8^{ab}	8.50±3.21^{a}	7.81±1.69^{ab}	7.2±1.03^{ab}	7.16±1.1^{ab}	7.1±0.94^{ab}	6.7±1.2^{b}
L3	F	7.43±2.05^{a}	7.91±1.23^{a}	8.32±1.15^{a}	8.01±1.35^{a}	7.82±1.25^{a}	7.57±0.67^{a}	7.97±1.42^{a}
	M	7.86±1.37^{ab}	7.97±1.29^{ab}	8.54±1.19^{a}	7.77±1.29^{ab}	7.29±1.33^{b}	7.51±1.08^{ab}	8.06±1.36^{ab}
L4	F	7.3±0.67^{a}	8.29±1.19^{a}	7.68±1.11^{a}	8.00±1.47^{a}	8.18±0.96$^{\#a}$	11.11±11.19^{a}	7.92±2.88^{a}
	M	7.35±1.12^{a}	8.08±0.95^{a}	7.94±1.66^{a}	7.57±1.31^{a}	7.35±0.76^{a}	7.1±1.3^{a}	7.98±1.61^{a}
L5	F	6.83±1.41^{a}	7.04±1.36^{a}	6.69±1.88^{a}	6.48±1.04^{a}	7.46±1.31^{a}	6.7±1.03^{a}	6.59±1.63^{a}
	M	6.73±1.50^{ab}	7.08±1.18^{ab}	6.51±1.16^{b}	6.72±0.93^{ab}	6.93±1.45^{ab}	6.72±1.18^{ab}	7.89±1.6^{a}

: male> female is significant (p<0.05)

Appendix 9 – Mean percentage deviations, for each parameter, between different combinations of imaging modalities, for Group 1 (8 patients).

Vertebra height (%)						
Vertebra	**MRI versus Standing X-ray**		**MRI versus Functional X-ray**			
			Extension		**Flexion**	
	Anterior	**Posterior**	**Anterior**	**Posterior**	**Anterior**	**Posterior**
L1	-30.65 ± 5.82	-34.13 ± 6.39	-30.61 ± 6.66	-35.70 ± 8.58	-33.84 ± 9.30	-34.77 ± 9.80
L2	-31.37 ± 9.30	-33.61 ± 10.06	-29.53 ± 6.59	-34.43 ± 6.52	-33.82 ± 9.97	-33.90 ± 9.52
L3	-30.54 ± 9.96	-34.08 ± 12.80	-29.21 ± 9.42	-33.91 ± 10.82	-25.96 ± 13.12	-36.64 ± 12.11
L4	-30.63 ± 7.34	-27.17 ± 13.13	-30.09 ± 7.60	-24.97 ± 10.66	-29.23 ± 9.90	-30.58 ± 10.03
L5	-33.19 ± 9.22	-28.10 ± 9.91	-32.72 ± 7.63	-29.14 ± 8.30	-31.19 ± 9.51	-28.31 ± 9.55
S1	-33.67 ± 10.93	-38.24 ± 9.00	-41.48 ± 10.37	-46.21 ± 11.63	-27.81 ± 12.91	-32.34 ± 10.22

IVD height (%)						
IVD	**MRI versus Standing X-ray**		**MRI versus Functional X-ray**			
			Extension		**Flexion**	
	Anterior	**Posterior**	**Anterior**	**Posterior**	**Anterior**	**Posterior**
L1-L2	-35.54 ± 18.56	-13.90 ± 16.65	-40.15 ± 19.93	-3.59 ± 20.34	-9.78 ± 16.11	-21.75 ± 14.84
L2-L3	-38.39 ± 12.82	-22.41 ± 23.34	-44.88 ± 17.43	-10.44 ± 24.15	-15.32 ± 12.41	-26.59 ± 27.24
L3-L4	-46.09 ± 20.21	-12.83 ± 24.08	-42.53 ± 16.10	-9.98 ± 23.56	-21.87 ± 23.54	-19.09 ± 15.86
L4-L5	-29.85 ± 18.26	-41.38 ± 42.68	-35.40 ± 23.49	-43.29 ± 51.24	-15.84 ± 25.18	-37.27 ± 47.22
L5-S1	-33.28 ± 12.02	-26.45 ± 28.16	-39.77 ± 14.05	-16.88 ± 28.10	-23.57 ± 15.99	-25.03 ± 27.47

Intervertebral angle (%)			
IVD	**MRI versus Standing X-ray**	**MRI versus Functional X-ray**	
		Extension	**Flexion**
L1-L2	-373.98 ± 384.73	-595.62 ± 841.37	-129.97 ± 198.32
L2-L3	-330.41 ± 475.08	-407.49 ± 522.94	-136.39 ± 309.05
L3-L4	-114.94 ± 185.59	-132.43 ± 198.70	-11.85 ± 57.39
L4-L5	-8.90 ± 33.38	-16.26 ± 39.08	32.42 ± 34.14
L5-S1	-9.83 ± 31.33	-50.00 ± 52.05	-7.93 ± 51.38

Lumbar lordosis angle (%)		
MRI versus Standing X-ray	**MRI versus Functional X-ray**	
	Extension	**Flexion**
-20.38 ± 11.28	-33.16 ± 15.27	20.17 ± 41.59

Appendix 10 – Mean percentage deviations, for each parameter, between different combinations of imaging modalities, for Group 2 (4 patients).

Vertebra height (%)					
Vertebra	**MRI versus CT**			**MRI versus Standing X-ray**	
	Anterior	**Central**	**Posterior**	**Anterior**	**Posterior**
L1	-8.19 ± 2.52	-7.34 ± 3.00	-18.89 ± 7.35	-30.32 ± 6.54	-35.33 ± 8.16
L2	-10.16 ± 3.40	-6.59 ± 1.91	-12.02 ± 6.07	-32.60 ± 12.48	-35.05 ± 12.60
L3	-8.01 ± 5.15	-7.40 ± 2.12	-12.33 ± 7.99	-30,67 ± 12.85	-34.38 ± 17.36
L4	-8.34 ± 2.56	-16.43 ± 8.40	-10.00 ± 4.96	-30.34 ± 7.99	-25,38 ± 17.31
L5	-6.02 ± 2.49	-7.92 ± 5.50	-3.47 ± 6.15	-33.55 ± 11.62	-23.13 ± 9.19
S1	-3.10 ± 2.10	-5.66 ± 7.41	-3.86 ± 6.04	-29.82 ± 10.00	-38.19 ± 3.73

Vertebra height (%)				
Vertebra	**MRI versus Functional X-ray**			
	Extension		**Flexion**	
	Anterior	**Posterior**	**Anterior**	**Posterior**
L1	-33.16 ± 5.74	-42.44 ± 5.36	-33.89 ± 10.38	-37.71 ± 11.65
L2	-29.07 ± 6.92	-34.40 ± 7.73	-37,28 ± 11.82	-35.90 ± 12.23
L3	-29.99 ± 11.74	-34.80 ± 14.28	-23.79 ± 16.97	-40.80 ± 15.69
L4	-31.34 ± 5.83	-25.31 ± 11.42	-29.86 ± 12.34	-31.25 ± 10.92
L5	-34.71 ± 8.23	-28.67 ± 8.10	-34.09 ± 10.79	-26.16 ± 10.99
S1	-41.89 ± 5.60	-49.56 ± 3.91	-24.83 ± 8.16	-33.93 ± 6.50

Vertebra height (%)			
Vertebra	**MRI versus 3D models**		
	Anterior	**Central**	**Posterior**
L1	-9.76 ± 3.06	-9.45 ± 4.63	-18.81 ± 5.55
L2	-11.80 ± 4.16	-12.07 ± 2.16	-12.32 ± 5.65
L3	-9.79 ± 6.89	-12.71 ± 1.98	-13.46 ± 7.15
L4	-12.01 ± 3.61	-18.17 ± 1.67	-11.42 ± 5.03
L5	-10.02 ± 2.99	-12.57 ± 9.01	-7.58 ± 6.14
S1	-5.23 ± 2.04	-10.53 ± 7.65	-5.52 ± 3.13

IVD height (%)					
IVD	**MRI versus CT**			**MRI versus Standing X-ray**	
	Anterior	**Central**	**Posterior**	**Anterior**	**Posterior**
L1-L2	29.21 ± 7.47	21.45 ± 3.27	55.99 ± 13.51	-24.04 ± 11.82	-16.81 ± 19.37
L2-L3	29.69 ± 10.42	20.07 ± 9.06	47.87 ± 12.89	-30.58 ± 11.13	-29.67 ± 21.30
L3-L4	4.18 ± 7.50	17.78 ± 4.25	38.29 ± 9.06	-60.84 ± 19.43	-32.91 ± 11.63
L4-L5	16.65 ± 10.93	24.93 ± 13.90	35.24 ± 7.49	-28.33 ± 6.36	-31.07 ± 12.71
L5-S1	19.57 ± 12.24	29.79 ± 6.97	31.90 ± 16.36	-35.30 ± 10.30	-37.88 ± 32.01

IVD height (%)				
IVD	MRI versus Functional X-ray			
	Extension		Flexion	
	Anterior	Posterior	Anterior	Posterior
L1-L2	-27.85 ± 9.00	-11.99 ± 22.40	-3.09 ± 14.22	-28.80 ± 14.86
L2-L3	-34.86 ± 11.42	-21.96 ± 26.68	-9.85 ± 13.78	-27.40 ± 24.91
L3-L4	-52.62 ± 14.87	-28.26 ± 18.71	-36.55 ± 22.90	-27.75 ± 13.38
L4-L5	-29.66 ± 2.11	-37.00 ± 21.31	-11.42 ± 11.84	-19.61 ± 22.84
L5-S1	-40.60 ± 5.11	-19.54 ± 34.07	-34.09 ± 7.82	-27.08 ± 13.05

IVD height (%)			
IVD	MRI versus 3D models		
	Anterior	Central	Posterior
L1-L2	33.89 ± 4.76	30.44 ± 2.63	58.31 ± 14.45
L1-L2	33.26 ± 11.77	30.52 ± 11.57	47.64 ± 15.48
L1-L2	12.09 ± 5.74	27.52 ± 2.02	47.53 ± 15.81
L1-L2	21.79 ± 10.31	29.01 ± 4.35	45.09 ± 6.35
L1-L2	25.31 ± 7.05	37.90 ± 9.85	40.86 ± 16.21

Intervertebral angle (%)					
IVD	MRI versus CT	MRI versus Standing X-ray	MRI versus Functional X-ray		MRI versus 3D models
			Extension	Flexion	
L1-L2	-104.52 ± 79.94	-130.06 ± 183.07	-70.25 ± 123.84	1.54 ± 68.55	-93.91 ± 100.49
L2-L3	-52.53 ± 74.90	-60.04 ± 102.64	-49.91 ± 104.01	31.47 ± 57.84	-47.45 ± 70.97
L3-L4	-135.93 ± 214.00	-163.42 ± 249.44	-160.15 ± 277.69	-22.65 ± 46.64	-141.14 ± 23.62
L4-L5	1.46 ± 30.32	-14.46 ± 44.78	-25.53 ± 50.08	32.97 ± 36.61	2.80 ± 27.80
L5-S1	-21.59 ± 28.09	-19.38 ± 36.77	-58.17 ± 27.84	-16.05 ± 12.65	-21.83 ± 34.50

Lumbar lordosis angle (%)				
MRI versus CT	MRI versus Standing X-ray	MRI versus Functional X-ray		MRI versus 3D models
		Extension	Flexion	
-7.45 ± 8.69	-18.19 ± 14.70	-24.05 ± 11.99	15.51 ± 40.36	-11.86 ± 10.93